Comparative Performance Evaluation of Carbon & Basalt Fiber Reinforced Copper Composites for Brake Pads in Armoured Fighting Vehicles

Utkarsh Chadha[1]*, Mayank Khanna[2], Divyansh Srivastava[3], Senthil Kumaran Selvaraj[4]*, Dhanalakshmi S[5]

[1]Department of Materials Science and Engineering, Faculty of Applied Sciences and Engineering, University of Toronto, St. George Campus, Toronto, Ontario, Canada, M5S 1A1

[2]University of Bath, Bath, United Kingdom

[3]Technische Universitat Darmstadt, Darmstadt, Germany

[4]Department of Manufacturing Engineering, School of Mechanical Engineering (SMEC), Vellore Institute of Technology (VIT), Vellore, Tamilnadu, India – 632014.

[5]Combat Vehicles Research & Development Establishment (CVRDE), Defence Research & Development Organization (DRDO), Ministry of Defence, Government of India, Avadi, Chennai, Tamilnadu, India – 600054.

*Corresponding: senthilkumaranselvaraj82@gmail.com: Utkarsh.chadha@mail.utoronto.ca;

Abstract

Armoured Fighting Vehicles (AFVs) usually require durable brake pads with lesser wear and longevity. However, the currently deployed Copper MMC-based brake pads do not fully complement the requirements for an AFV. With the need for innovation, this research provides various recipes of brake pads with varying quantities of carbon or basalt reinforcement ranging from 0.25 wt% to 1.25%. However, the currently available literature does not provide sufficient evidence for using Basalt Fiber & Carbon fiber and the possible effects within an AFV's environment. So, the formulations were tested, and compressed into green compact pin samples for experiments after sintering, like Vickers' hardness test, Pin on Disc Wear Test, SEM analysis, EDX, and XRD analysis for validation. Additionally, modeling and simulation for brake pads and their assembly were done for 1.5 to 5 tonnes of load. This research provides a comparative study between Carbon and Basalt Fibers based copper samples for brake pad applications and high-performance applications like Armoured Fighting Vehicles.

Keywords: Copper Metal Matrix, Carbon Fiber, Basalt Fiber, Powder Metallurgy, Sintering, SEM analysis, Reinforcements, Armoured Fighting Vehicles, Heavy-Duty Vehicles

1. Introduction

Brake pads convert a vehicle's kinetic energy to heat energy through friction. The brake has two pads, one on each side of the rotor, facing the rotor's friction surfaces. The caliper clamps or squeezes the two pads onto the spinning rotor when the brakes are applied hydraulically to slow and stop the vehicle [1-3]. When a brake pad warms up from contact with the rotor, minute quantities of friction material are transferred to the disc, producing a dull grey covering. The friction material on the brake pad and disc "stick" to each other, generating friction that stops the vehicle [4-6]. In disc brakes, each disc rotor typically has two brake pads. A caliper

mounted to the wheel hub or suspension upright holds these in position and activates them. Racing calipers can use up to six pads with various frictional qualities when placed in a staggered pattern for best performance [7].

Dhanalakshmi S et al. (2007) investigated the sintered copper brake pads and found their performance appropriate, even during wet friction. The composition used contained Sn (4-6%), Multite (5.5-8.5%), Graphite (4.5-7.5%), along with Copper [8]. Peng Zhang et al. (2019) added Al_2O_3, which significantly reduced wear loss of the brake pad; the relationship between braking properties and tribo-film was assessed in the research [9]. Peng Zhang et al. (2020) further investigated the incorporation of 0-1.2% of the 0.4% Carbon fiber samples in the experiments obtain the best wear performance. The samples incorporated Cementite with Fe particles were utilized as the friction coefficient stabilizer [10]. Further investigating the copper brake pads, it was found that they should have appropriate oxidation resistance in the temperature range of 400-800°C to perform for a prolonged period in a commercial and heavy vehicle environment [11]. In [11], the investigation involved granular & flake Graphite, Ferrochrome (FeCr), which acts as a friction coefficient stabilizer, Silicon Carbide, and Iron [12, 13]. Figure 1 shows the basics of a brake pad and what are the expected properties and performance expectations of a brake pad being developed

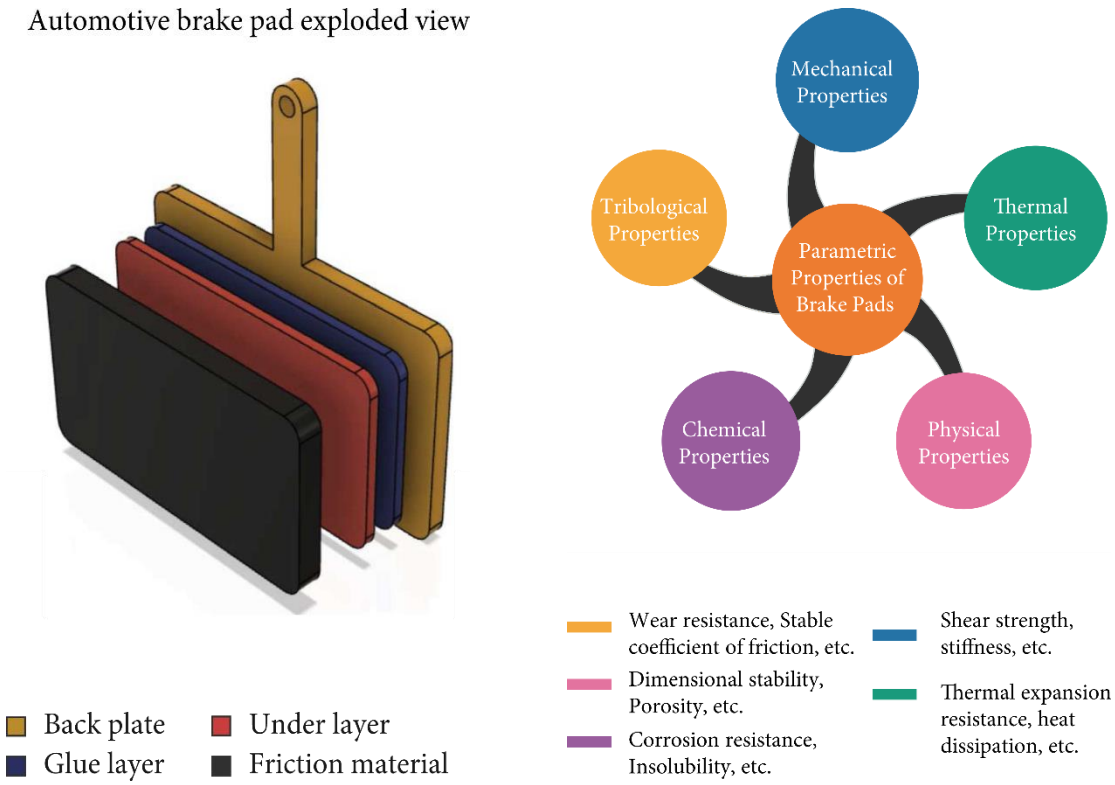

Figure 1. General Brake Pad (a) Layout, (b) Desired Properties [14]

This study provides vital insight regarding the investigations conducted to date and the gaps this research fulfills regarding possible alternative materials apart from traditionally brake pads have been scarcely explored, consisting of a Copper matrix, a solid lubricant. Secondly,

Ferrochrome as a friction coefficient stabilizer in brake pads has not been studied extensively in defense applications, alongside decreasing the Molybdenum content compared to the commercially used brake pads. Although Carbon reinforcement could be found, a negligible amount of literature is available on using Basalt Fiber reinforcement. Furthermore, currently available literature on Defence oriented brake pads is inaccessible or very limited; hence is not readily available. In heavy vehicles, investigations have been conducted for high-speed trains or commercial automotive vehicles [14].

"Barites, mica, Allium sativum, and cashew dust are a few of the most popular alternatives being studied for use as filler material" Selvaraj et al. (2021) [14]. However, comparatively, investigations have not been conducted for the brake pads, and this research mainly provides a fibers-related comparative analysis of Carbon and Basalt Fiber based copper brake pads.

2. Materials

Metals Used

We have taken metal powders and mixed them in a fixed proportion constituting 62% Cu with Carbon or Basalt fiber, Silicon Carbide (SiC), Boron Nitrate (BN), Molybdenum Disulphide (MoS_2), and Ferrochrome (FeCr) (Shiny Iron Powder) (Figure 1).

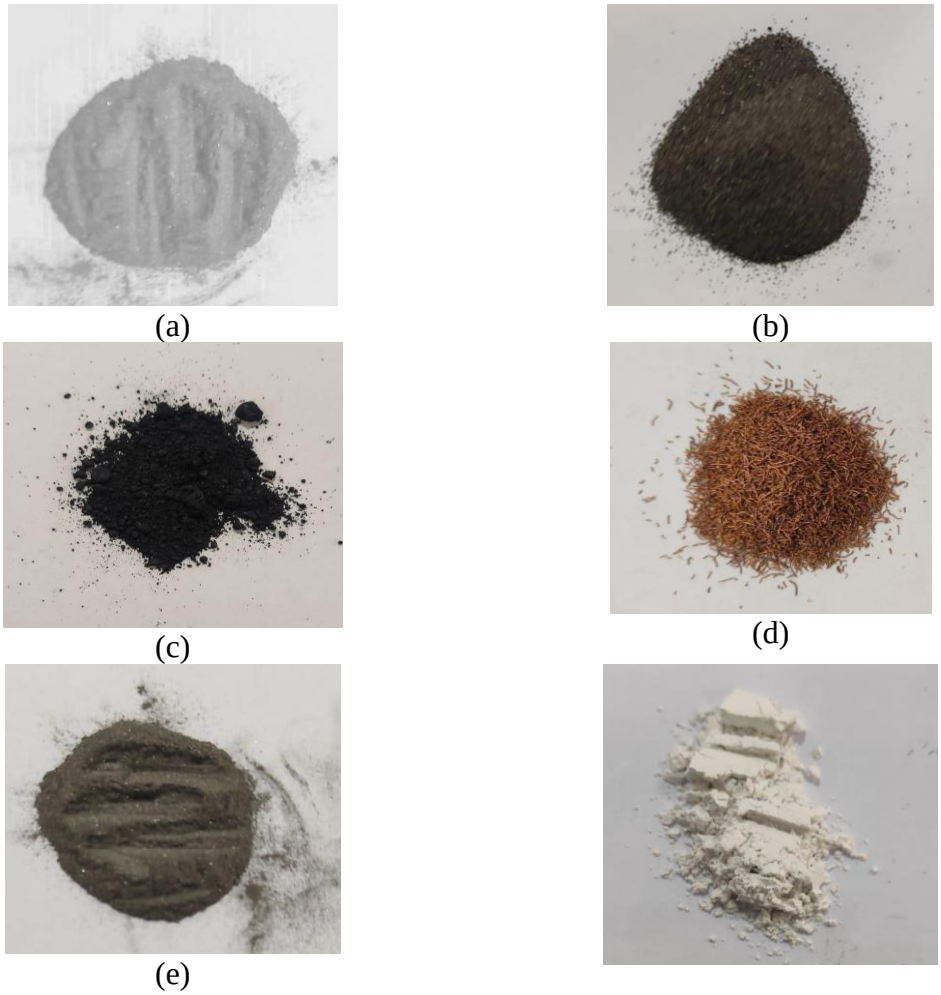

(a) (b) (c) (d) (e)

(f)

Figure 2. Powders Used for Brake Pad Recipe (a) SiC, (b) Fe^{+2}, (c) MoS_2, (d) Cu, (e) FeCr, (f) Hydroxyapetite.

From Figure 2, the Materials Selected are as follows:

(1) Fe: It is added to stabilize the friction coefficient and enhance wear properties [15].
(2) SiC: Excessive SiC addition will also cause a composite's failure, as it may compromise the ductility. The addition of silicon carbide in a limited amount (up to 10wt%) also reduces surface wear [16].
(3) BN: Its tight hexagonal lattice of alternating boron and nitrogen atoms is highly resistant to change, unlike graphene and other 2-D materials that can be easily modified—aka functionalized—with other elements [17].
(4) MoS_2: It acts as a lubricating agent to fill the macropores of the material [18]. It has an adjusting property to fill the porosity throughout the matrix and is added 1-2% in the usual case [18].
(5) Cr–Fe: the size of a few hundred micrometers in powder metallurgy pads (PM Pads) were found to be embedded in the iron matrix. It has been reported that the Cr–Fe particles in PM brake materials usually play the role of increasing friction effect in place of just adding pure chromium. The Fe included in the composite is easily mixed in the FerroChrome Matrix, enhancing the overall friction coefficient [19].
(6) Cu: Copper has long been used in many friction materials because it is a good conductor of heat. It helps cool the brake pads, stabilizing the friction characteristics for more consistent braking and reduced fade. It also helps reduce noise [20].

Fibers Used

The fibers used in this experiment were Carbon and Basalt Fibers (Figure 3). The fibers were taken in fixed quantities in the Cu MMC. These fibers were reinforced in the Cu MMC for further sample making, and testing.

(a)

(b)

Figure 3. The Fibers. (a) Carbon Fiber, (b) Basalt Fiber.

3. Experimentations

Mixing of Fibers & Powders

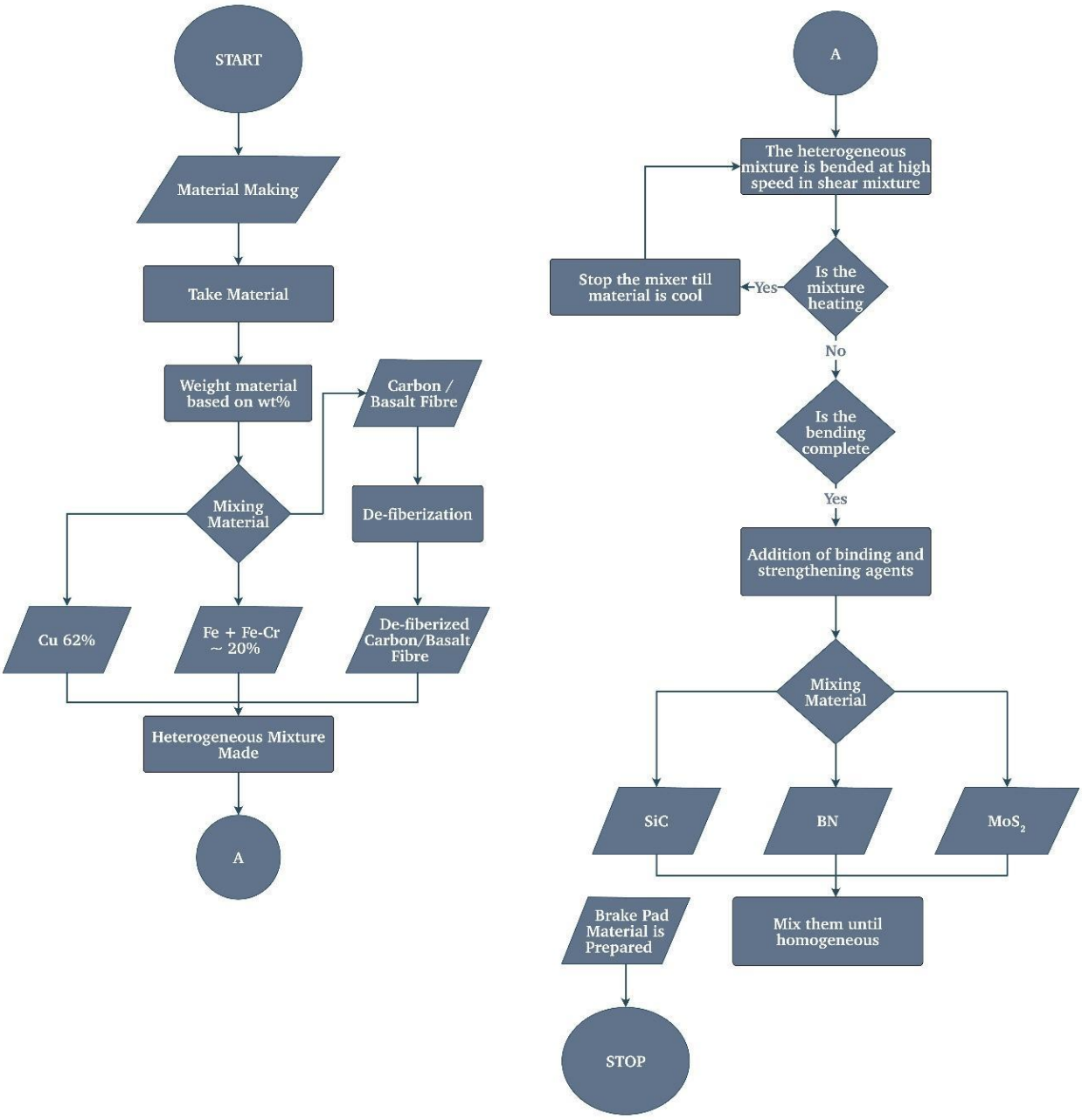

Figure 4. Mixing of Powders & Fibers for the Brake pad recipe.

Figure 4 explains the whole process of mixing the powders and fibers. The procedure involves de-fiberizing Carbon and Basalt Fiber separately in a mixture machine (Figure 5). We had increased the speed to 160-180 rpm for 10 mins. When mixed Cu, Fe, and FeCr, we reduced the mixer's speed to 80 rpm.

Figure 5. Mixture Machine with Speed Adjuster.

We added SiC and 7-8% of BN, and after these additions, we added MoS_2 for Flowability and Texture. The whole recipe is shown in Table 2 for Carbon Fiber and Table 3 for Basalt Fiber with a detailed list of elements mixed in fixed proportions. We have checked the process every 30 mins if the powder was not stuck and was mixed appropriately to maintain the homogeneity of the mixture and avoid its sticking to the surface of the powder mixing machine. For 6 cycles, comprising 3 hours for the whole process, each powder sample underwent the process, and we have prepared 6 such powders with fixed percentages of Carbon and Basalt as applicable. Figure 5(a), (b), and (c) show a visual representation of the selected compositions in Table 1, 2.

Table 2. Brake Pad Recipe Using Carbon Fiber.

Formation 1: Carbon fibre 0.25 wt%			
S.no.	Material	wt%	wt for 350gms
1	Cu	62	217
2	Fe^{2+}	8	28
3	CrFe	10	35
3	SiC	7	24.5
4	BN	10	35
5	MoS_2	2.75	9.625
6	C-Fiber	0.25	0.875
	total	100	350

Formation 2: Carbon fibre 0.75 wt%

S.no.	Material	wt%	wt for 350gms
1	Cu	62	217
2	Fe^{2+}	8	28
3	CrFe	10	35
3	SiC	7	24.5
4	BN	10	35
5	MoS_2	2.25	7.875
6	C-Fiber	0.75	2.625
	total	100	350

Formation 3: Carbon fibre 1.25 wt%			
S.no.	Material	wt%	wt for 350gms
1	Cu	62	217
2	Fe^{2+}	8	28
3	CrFe	10	35
3	SiC	7	24.5
4	BN	10	35
5	MoS_2	1.75	6.125
6	C-Fiber	1.25	4.375
	total	100	350

Table 3. Brake Pad Recipe Using Basalt Fiber.

Formation 1: Basalt fibre 0.25 wt%			
S.no.	Material	wt %	wt for 350gms
1	Cu	62	217
2	Fe^{2+}	8	28
3	CrFe	10	35
3	SiC	7	24.5
4	BN	10	35
5	MoS_2	2.75	9.625
6	B-Fiber	0.25	0.875
	total	100	350

Formation 2: Basalt fibre 0.75 wt%			
S.no.	Material	wt %	wt for 350gms

1	Cu	62	217
2	Fe^{2+}	8	28
3	CrFe	10	35
3	SiC	7	24.5
4	BN	10	35
5	MoS_2	2.25	7.875
6	B-Fiber	0.75	2.625
	total	100	350

Formation 3: Basalt fibre 1.25 wt%			
S.no.	Material	wt %	wt for 350gms
1	Cu	62	217
2	Fe^{2+}	8	28
3	CrFe	10	35
3	SiC	7	24.5
4	BN	10	35
5	MoS_2	1.75	6.125
6	B-Fiber	1.25	4.375
	total	100	350

Manufacturing of Pin Samples

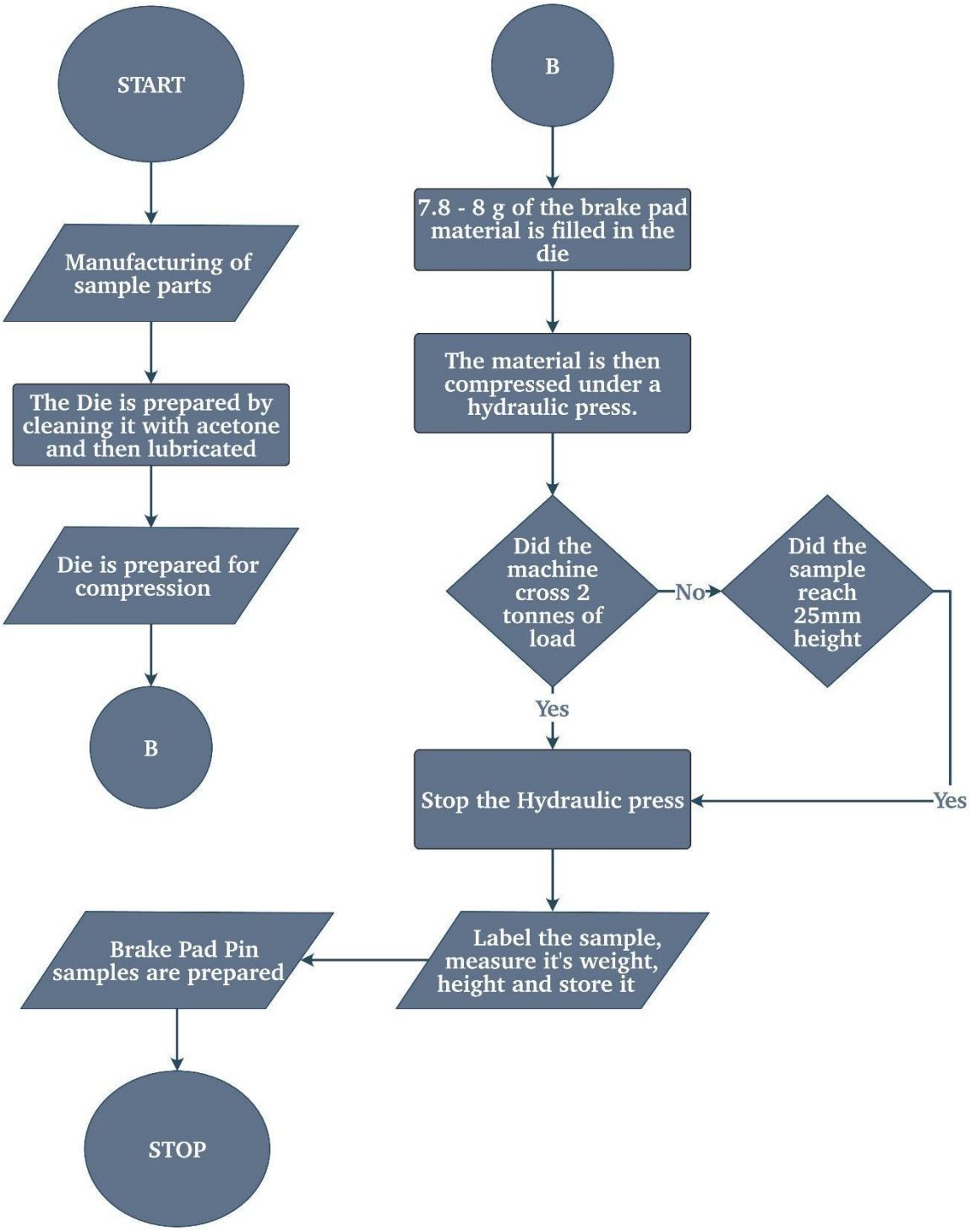

Figure 6. Manufacturing of Pins.

The powder is taken in approximately 7-8 g amounts for the desired sample inside a die. The plunger is marked using a marker for 35 mm and 40 mm measurements and keeping track of compaction under the hydraulic press only for reference since a bottom punch of 10 mm is added. The desired height for green compact samples was required to be 25 mm. A 10 mm

bottom punch is kept below inside the die for appropriate compression into a green compact to ensure the powder does not come out of the die (Figure 6). Approximately 60 green compact samples were made after the compaction in the hydraulic press for further testing. The samples and their heights, indicator value of the hydraulic press, initial & final weights of the obtained pin samples, density (Initial & Final), and porosity for Cabon & Basalt Fiber samples in 0.25wt%, 0.75wt%, and 1.25wt% have been provided in Table 4, 5.

The calculations performed in Tables 4, 5 are using the below equations:

$$Density = \frac{Weight\ of\ Pin}{\pi * radii^2 * Height\ of pin} \quad (1)$$

$$\Delta porosity = 1 - \frac{After\ sintering\ weight}{Before\ sintering\ weight} \quad (2)$$

$$Pressure\ applied\ (Mpa) = \frac{Force\ (kg) * 9.8}{\pi * radii^2} \quad (3)$$

Table 4. Evaluation of Carbon Fiber Pin Samples. (Attached Separately)

Carbon fiber
0.25wt%

S.no.	wt. of powder	Indicator value	Weight of Pin		Height of Pin		sintering	Density		porosity	re-sizing	Micro hardness	force (tone)	pressure (Mpa)
			before sintering	after sintering	before sintering	after sintering		before	after					
1	7.8	15.2	7.9		23.68			4.250					1.17	145.967663
2	7.8	9	7.8		24.78			4.010					0.69	86.4282215
3	7.8	8.5	7.8		25.04			3.968					0.65	81.6266536
4	7.7	8	7.6		25.04			3.866					0.62	76.8250857
5	7.8	8.3	7.8	6.95	25.22	25.84	*	3.940	3.426	0.130353457	Y		0.64	79.7060265
6	7.8	10.5	7.8		23.78			4.178					0.81	100.832925
7	7.8	8	7.8	6.91	25.44	25.9	*	3.906	3.399	0.12983665			0.62	76.8250857
8	7.8	8.5	7.8		25.1			3.959					0.65	81.6266536
9	7.8	9.1	7.7		25.88			3.790					0.70	87.388535
10	7.7	8.7	7.7	7.11	25.76	26.56	*	3.808	3.410	0.104435926		Y	0.67	83.5472807

Carbon fiber
0.75wt%

S.no.	wt. of powder	Indicator value	Weight of Pin		Height of Pin		sintering	Density		porosity	re-sizing	Micro hardness	force (tone)	pressure (Mpa)
			before sintering	after sintering	before sintering	after sintering		before	after					
1	7.6	16.2	7.6		22.84			4.239					1.25	155.570799
2	7.7	10.8	7.7		25.08			3.911					0.83	103.713866
3	7.8	9.7	7.8	7.01	25.18	25.64	*	3.946	3.483	0.117405696		y	0.75	93.1504165
4	7.8	11.1	7.7		24.88			3.942					0.85	106.594806
5	7.8	9.1	7.8	7.12	25.68	25.8	*	3.869	3.516	0.091425164	y		0.70	87.388535
6	7.8	10	7.8	7.01	25.78	25.58	*	3.854	3.491	0.094255328			0.77	96.0313572
7	7.9	9.9	7.9		25.5			3.947					0.76	95.0710436
8	7.8	10.3	7.8		25.5			3.897					0.79	98.9122979
9	7.8	9.8	7.8		25			3.975					0.75	94.11073
10	7.8	22.2	7.8		22.85			4.348					1.71	213.189613

Carbon fiber 14/03/20
1.25wt% 22

S.no.	wt. of powder	Indicator value	Weight of Pin		Height of Pin			Density		porosity	re-sizing	Micro hardness	force (tone)	pressure (Mpa)
			before sintering	after sintering	before sintering	after sintering		before	after					
1	7.8	10.2	7.9		25.56			3.937					0.78	97.9519843
2	8	11.4	8		25.88			3.938					0.88	109.475747
3	7.7	10.9	7.6	7.06	23.56	24.88	*	4.109	3.615	0.120337621	y		0.84	104.674179
4	7.8	10.1	7.7		25.02			3.920					0.78	96.9916707
5	7.8	9.7	7.8	6.95	25.64	26.98	*	3.875	3.282	0.153228412		y	0.75	93.1504165
6	7.8	13.5	7.8		24.38			4.076					1.04	129.642332
7	7.8	9	7.9		26.22			3.838					0.69	86.4282215

8	7.9	10.2	7.8		25.88			3.839					0.78	97.9519843
9	7.8	9.4	7.8	6.88	25.56	26.82	*	3.887	3.268	0.159387369			0.72	90.2694757
10	7.8	9	7.8		26.18			3.795					0.69	86.4282215

Legends:

y- *The sample was used for sintering*

*-*Sintered Samples*

Table 5. Evaluation of Basalt Fiber Pin Samples. (Attached Separately)

Basalt fiber
0.25wt%

S.no.	wt. of powder	Indicator value	Weight of Pin		Height of Pin		sintering	Density		porosity	re-sizing	Micro hardness	force (tonnes)	pressure (Mpa)
			before sintering	after sintering	before sintering	after sintering		before	after					
1	7.8	8.9	7.5		25.06			3.813					0.68	85.4679079
2	7.8	10.7	7.7		25.1			3.908					0.82	102.753552
3	7.9	11	7.7		24.46			4.010					0.85	105.634493
4	7.8	9.6	7.7	6.94	25.64	24.12	*	3.826	3.665	0.041903039			0.74	92.1901029
5	7.8	9.4	7.8	6.98	25.74	24.08	*	3.860	3.693	0.043438538	y		0.72	90.2694757
6	7.8	12.7	7.7		24.74			3.965					0.98	121.959824
7	7.8	9	7.8		25.82			3.848					0.69	86.4282215
8	7.8	10.2	7.7		25.62			3.829					0.78	97.9519843
9	7.8	10.2	7.8	7.06	25.64	24.14	*	3.875	3.726	0.038629363		Y	0.78	97.9519843
10	7.8	11.5	7.8		25.08			3.962					0.88	110.436061

Basalt fiber
0.75wt%

S.no.	wt. of powder	Indicator value	Weight of Pin		Height of Pin		sintering	Density		porosity	re-sizing	Micro hardness	force (tonnes)	pressure (Mpa)
			before sintering	after sintering	before sintering	after sintering		before	after					
1	7.9	10.8	7.8		24.56			4.046					0.83	103.713866

2	7.8	24	7.8		22.22			4.472					1.85	230.475257
3	7.86	11.2	7.83		26.02			3.833					0.86	107.55512
4	7.86	14	7.85	7.36	25.36	25.34	*	3.943	3.700	0.061680382			1.08	134.4439
5	7.84	10.8	7.79		26.04			3.811					0.83	103.713866
6	7.82	13.7	7.52		24.54			3.904					1.05	131.562959
7	7.82	10.4	7.82		26.08			3.820					0.80	99.8726115
8	7.88	17.1	7.84		24.6			4.060					1.32	164.213621
9	7.96	16.1	7.94	7.5	25.26	25.88	*	4.004	3.692	0.078044764	y		1.24	154.610485
10	7.87	11.9	7.84	7.37	25.78	26.14	*	3.874	3.592	0.072895359		Y	0.92	114.277315

Basalt fiber
1.25wt%

S.no.	wt. of powder	Indicator value	Weight of Pin		Height of Pin		sintering	Density		porosity	re-sizing	Micro hardness	force (tonnes)	pressure (Mpa)
			before sintering	after sintering	before sintering	after sintering		before	after					
1	7.87	15.9	7.8	7.33	25.94	26.12	*	3.830	3.575	0.066732438		Y	1.22	152.689858
2	7.85	20.8	7.83		25.02			3.987					1.60	199.745223
3	7.85	15.1	7.8	7.33	26.2	26.18	*	3.792	3.567	0.059538501	y		1.16	145.007349
4	7.86	17.3	7.78	7.31	25.46	25.66	*	3.893	3.629	0.067734684			1.33	166.134248
5	8.53	18.9	8.5		27.78			3.898					1.45	181.499265
6	8.58	18.7	8.53		27.86			3.900					1.44	179.578638
7	8.55	20.5	8.4		26.06			4.106					1.58	196.864282

Legends:

Y- The sample was used for Microhardness test

y- *The sample was used for sintering & resizing after sintering*

**-Sintered Samples*

VIT 15 TONE AUTOMATIC PRESS CALCULATION

LOAD IN TONNE	AREA=31.4CM2 BORE DIA - 100MM	LOAD IN KGS	PRESSURE IN KG/CM2	
1	78.5	1000	13	
2	78.5	2000	25	
3	78.5	3000	38	
4	78.5	4000	51	
5	78.5	5000	64	
6	78.5	6000	76	
7	78.5	7000	89	11
8	78.5	8000	102	12
9	78.5	9000	115	13
10	78.5	10000	127	15
11	78.5	11000	140	17
12	78.5	12000	153	19
13	78.5	13000	166	30
14	78.5	14000	178	43
15	78.5	15000	191	
16	78.5	16000	204	

(a) (b)

Figure 7. (a) Hydraulic Press and (b) its indicator value calculation sheet.

This system (powder, bottom punch, die, and plunger) is then taken to a hydraulic press for compression. In the hydraulic press, we set an indicator value of 26, equivalent to 2 Tonnes, as provided in the manual for the press (Figure 7 (a), (b)). The samples we pressed were under 1-1.5 Tonnes of 250 Mpa. This pressure is appropriate based on the literature, and pressure value may influence the outcomes visibly.

After compression, the material will be kept for some time to settle down. After 2-3 minutes, we use the ejection system (a hollow metal tool with a circular shape, which is similar to the die's dimensions) to remove the bottom punch and press the system under the hydraulic press in 2 iterations, the second iteration being for removal of the 'green compact' sample (Figure 8).

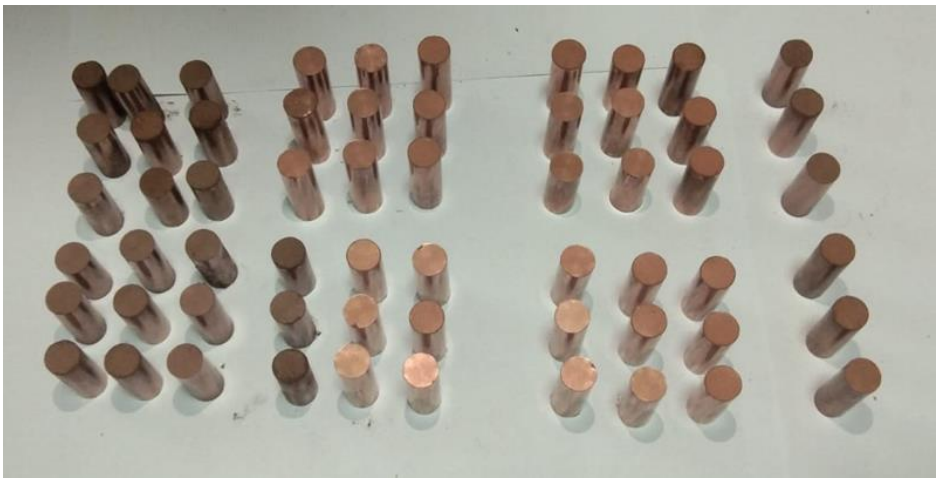

Figure 8. The Green Compact Samples.

We convert the indicator value (as shown in Figure 7(b)) provided in the manual for the hydraulic into tonnes, which are then converted into Newtons, and divide the area of the pin sample (10 mm diameter) to obtain the pressure. The obtained value is 78.5, divided by the factor obtained using the indicator value from the manual for the indicated amount of pressure.

Sintering Process

Figure 9. Tubular Furnace.

We set our green compact samples (samples undergone compaction only 1 time before sintering) and heated the sample at 925°C for sintering in a tubular furnace (Figure 9). The total time for the process was 7.5 hours, where 3 hours were consumed in the heating process in the Tubular Furnace. The crucibles contained all the green compact samples kept inside the tubular furnace. 2.5 hours were consumed for heating the furnace to 925°C (Figure 10).

Figure 10. Sintered Samples in the crucible.

The rising of the temperature was controlled to 5°C/min. 1.5 hours for temperature stabilization during the sintering process, where slag, moisture, and porosity are maximally removed. There was a reported black deposition, mainly due to the high temperature inside the Tubular Furnace (Figure 9).

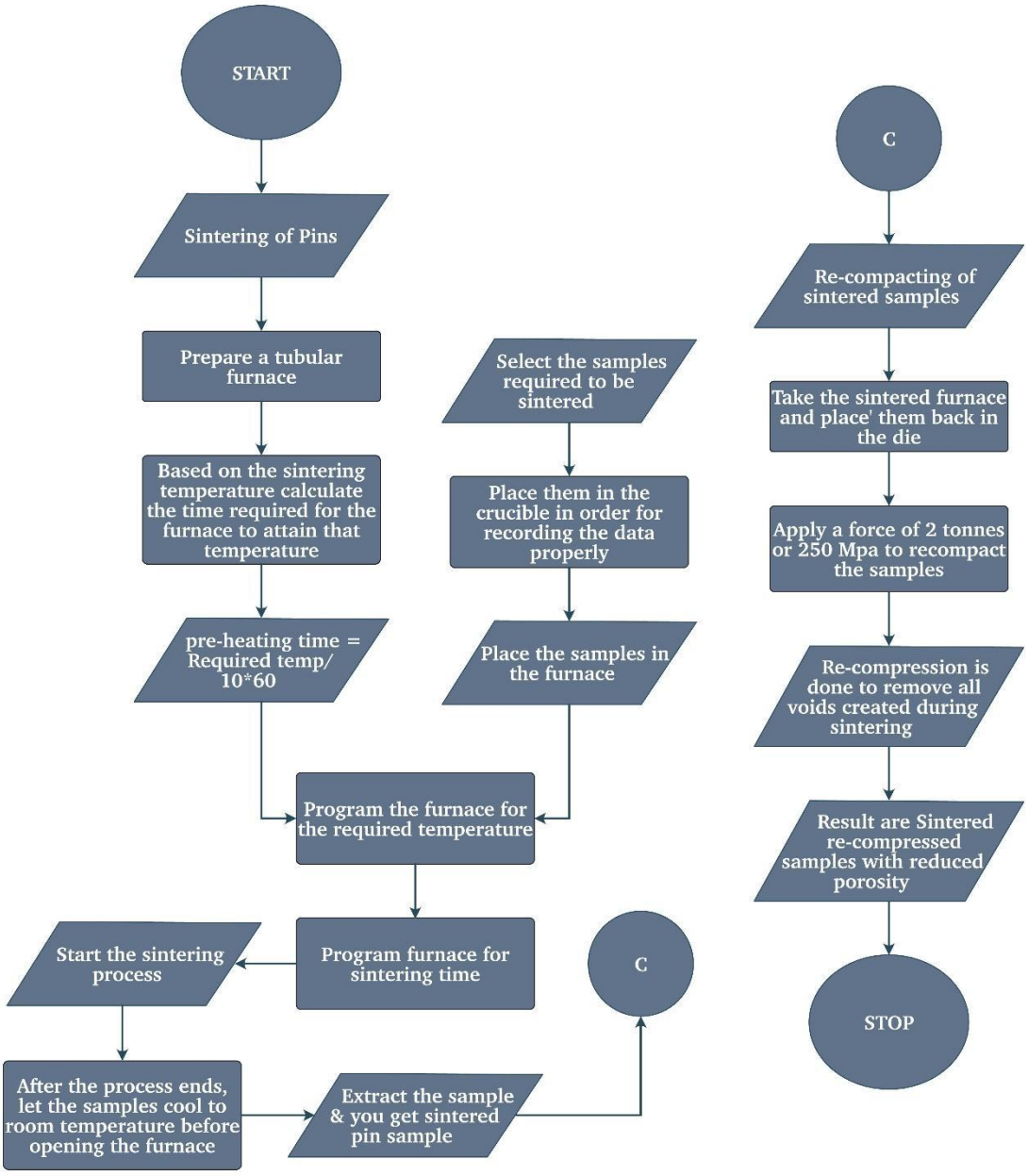

Figure 11. Sintering Process & Re-compaction after Sintering of Samples.

After sintering, the green compact samples are hardened, but the porosity is retained due to the water molecules or slag present in the sample. This porosity is removed by re-compaction of the samples under a hydraulic press (Figure 11).

Nitrogen flows at a very high rate within the furnace to maintain a Nitrogen atmosphere for the sintering process to occur, which is done to avert any surface roughness. According to various research, Argon and other similar gases may encourage surface roughness when their flow rate is high due to their heaviness compared to Nitorgen's usage. Cu has an FCC structure, and in an N_2 environment, a cubic phase is favoured. However, taking the Argon environment will promote the Hexagonal phase, which is unsuitable for sintering Cu [21, 22].

4. Results and Discussions: Testing of Samples & Outcomes

4.1. Material Characterization

4.1.1. SEM & EDX Analysis

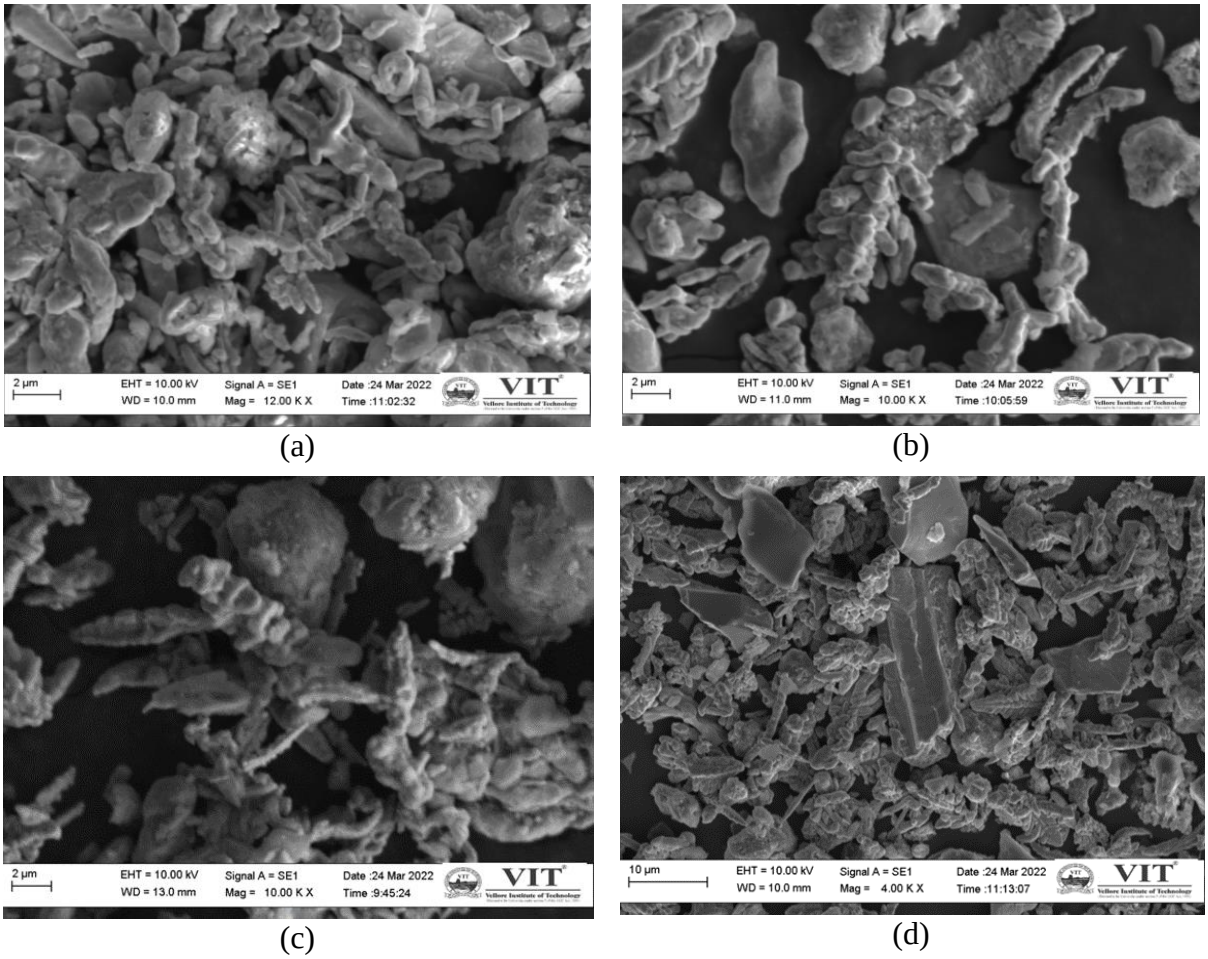

Figure 12. SEM Analysis of the Extreme Samples (a) Carbon Formation: 0.25wt%, (b) Basalt Formulation: 0.25wt%, (c) Carbon Formation: 1.25wt%, (d) Basalt Formulation: 1.25wt%.

The SEM analysis for the samples was conducted using Carl Zeiss EVO/18, with a magnification of 4000-12000X, at 10000V. Figure 12 shows the microstructures of the sintered green compact samples, after one iteration, before re-compaction. There were 4 samples taken for the SEM analysis, which were the extremes of both Carbon & Basalt Fiber samples, 0.25wt% and 1.25wt% samples. The microstructure obtained is evident in the fibers and dendritic growth on the surfaces.

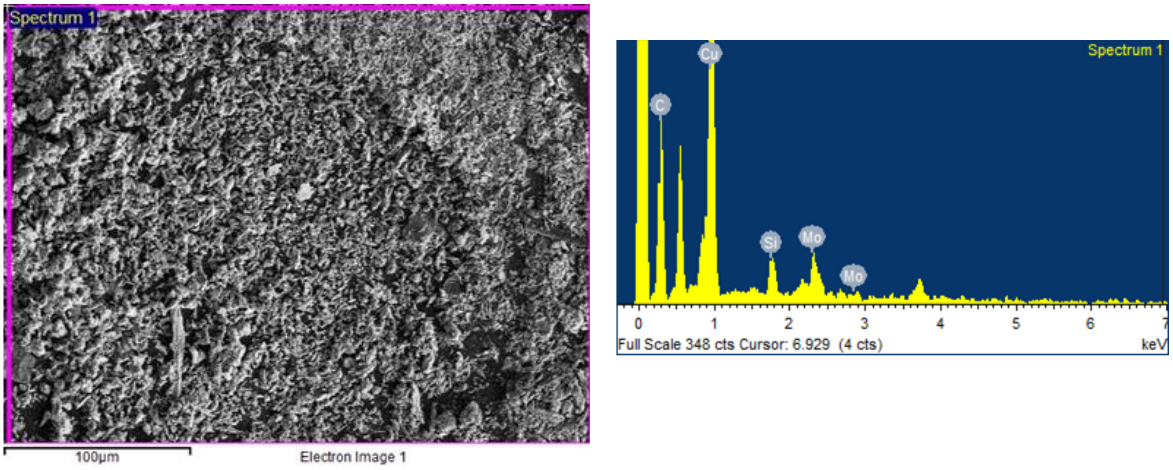
Spectrum 1
100µm
Electron Image 1
Spectrum 1
Cu
C
Si
Mo
Mo
0 1 2 3 4 5 6 7
Full Scale 348 cts Cursor: 6.929 (4 cts)
keV

(a)

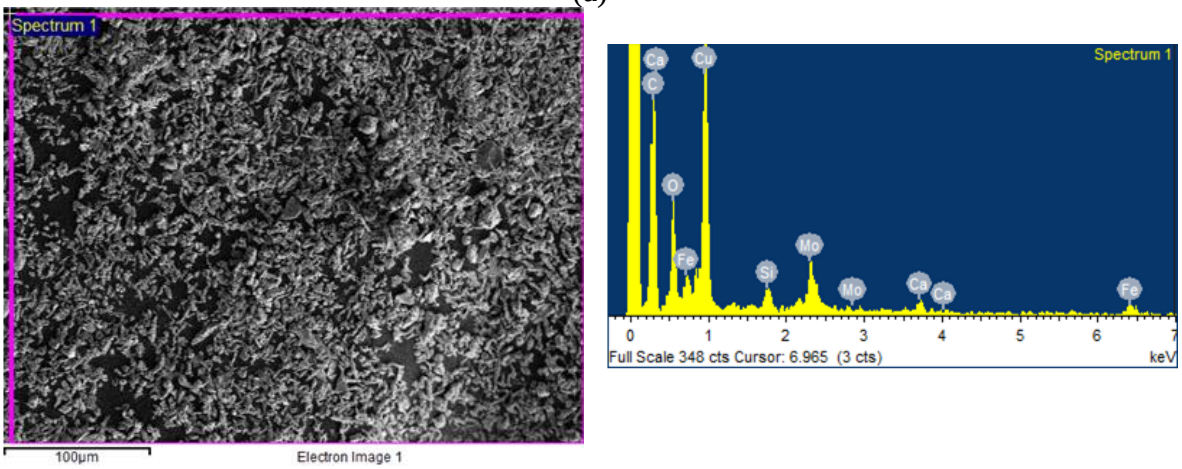
Spectrum 1
100µm
Electron Image 1
Spectrum 1
Ca
Cu
C
O
Fe
Si
Mo
Mo
Ca
Ca
Fe
0 1 2 3 4 5 6 7
Full Scale 348 cts Cursor: 6.965 (3 cts)
keV

(b)

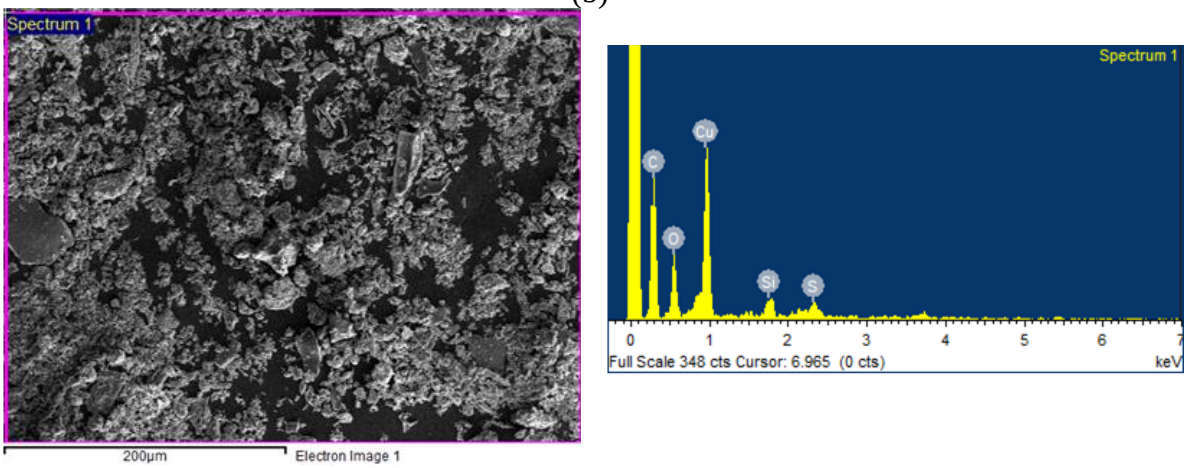
Spectrum 1
200µm
Electron Image 1
Spectrum 1
Cu
C
O
Si
Si
0 1 2 3 4 5 6 7
Full Scale 348 cts Cursor: 6.965 (0 cts)
keV

(c)

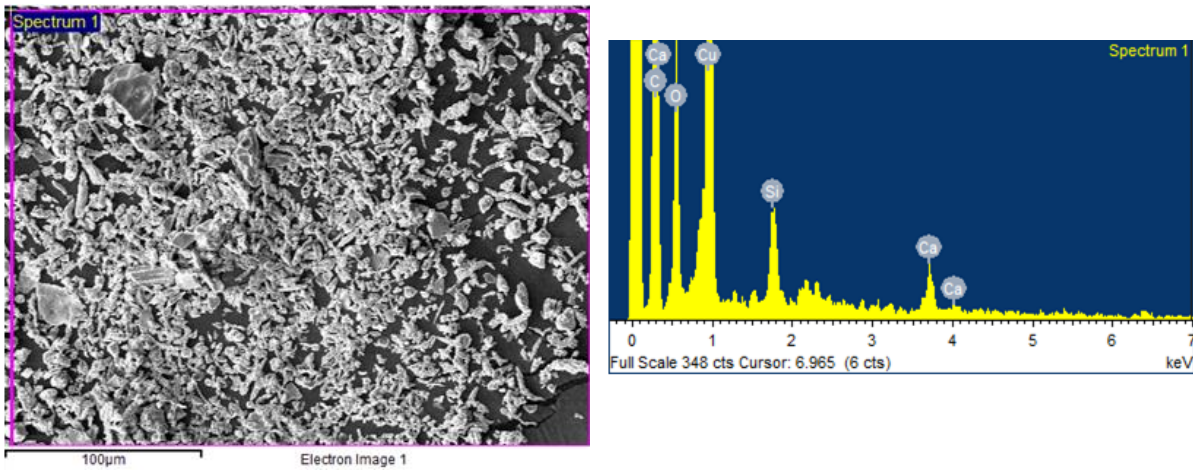

(d)

Figure 13. Energy Dispersive X-ray (EDX) Analysis of the Fiber Reinforced Samples. (a) Carbon 1.25%wt, (b) Basalt 0.25wt%, (c) Carbon 0.25wt%, (d) Basalt 1.25wt%

Figure 13 shows the Energy Dispersive X-Ray (EDX) Analysis of the Carbon and Basalt Fibers. A preliminary XRF test was conducted to investigate the elemental composition of the powder samples used for further preparation of the green compact samples before SEM & EDX analyses. Tables 6 to 8 list the elemental composition for each sample obtained in the EDX analysis.

Table 6. EDX elemental composition for Basalt 0.25wt% (Figure 13 (b))

Element	Weight%	Atomic%
C K	36.67	66.52
O K	11.26	15.33
Si K	1.15	0.89
Ca K	1.71	0.93
Fe L	10.28	4.01
Cu L	30.06	10.31
Mo L	8.88	2.02
Total		100

Table 7. EDX elemental composition for Carbon 0.25wt% (Figure 13 (c))

Element	Weight%	Atomic%
C	43.12	68.52

O	14.41	17.19
Si	2.36	1.60
S	2.16	1.29
Cu L	37.94	11.39
Total		100

Table 8. EDX elemental composition for Basalt 0.25wt% (Figure 13 (d))

Element	Weight%	Atomic%
C	36.75	62.79
O	15.52	19.90
Si	2.91	2.12
Ca	3.72	1.90
Cu L	41.11	13.28
Total		100

4.1.2. XRD Analysis

The X-Ray Diffractometer analysis was conducted using Bruker D8 Advance, Germany, with source being 2.2KW Cu anode, Ceramic X-Ray Tube. Theere were 6 samples tested, 3 for carbon fiber samples (0.25wt%, 0.75wt%, 1.25wt%), and Basalt Fiber (0.25wt%, 0.75wt%, 1.25wt%) in powder form. The values obtained for 2Θ were then processed using OriginLab software to obtain the graphs. The peaks obtained are verified, as shown in Figure 14 (a, b). An X-ray tube is generating monochromatic intensity of Cu Kα radiation in the 10° to 80° range at a scan speed of 5°/min. The generator is working at 40 kV and 30 mA. FWHM and peak analysis helps in determining the crystallite size using Scherer's formula which is given in Equation (4), and crystalline index of the cellulose region was determined using multiple peak fit analysis and Segal empirical equation which is given in Equation (5) where Scherrer's constant is given by K = 0.89 and λ is the wavelength of the radiation and β is the peak's full width at half-maximum [23].

$$\text{Crystallite Size } (L) = K/\beta\cos\theta \quad (4)$$

$$\text{Crystallinity Index} = ((I_{200} - I_{amorphous})/ I_{200}) \times 100 \quad (5)$$

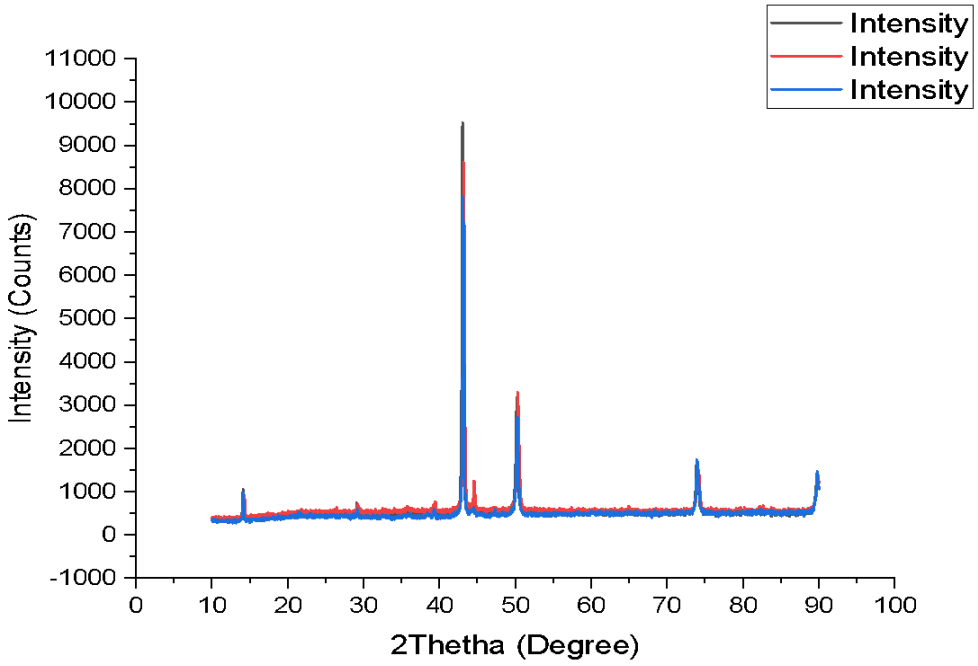

(a)

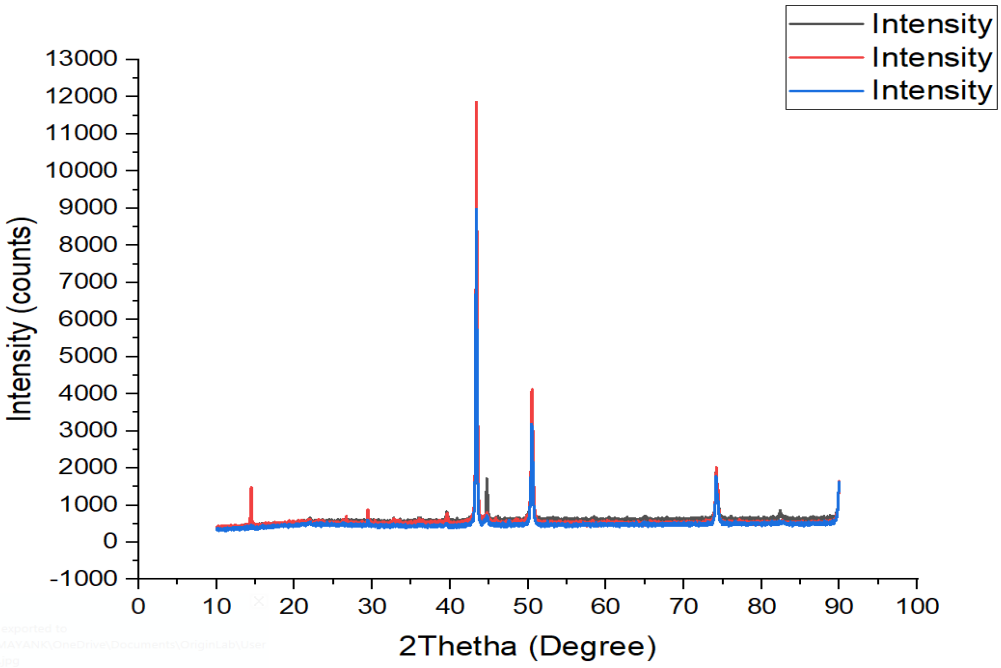

(b)

Figure 14. XRD Analysis Graph (Intensity vs. 2Θ), (a) Carbon Fiber Samples, (b) Basalt Fiber Samples.

4.2. Vicker's Hardness Test

(a) (b)

Figure 15. (a) Vickers hardness tester, (b) Test Screen.

The Vickers hardness test was conducted for all the 6 samples for Carbon & Basalt fibers, using a Matsuzawa Vickers Hardness Tester (Figure 15). Equation (6) was used for further calculations which are shown in Tables 9 to 14.

$$Vickers' Hardness\ (Gpa) = 0.1891 * \frac{Force}{(2*radii)^2} \quad (6)$$

Table 9. Vickers Hardness Test for Carbon 0.25wt% Sample.

Statistics Data										
Point	Max.	Min.	R	Ave.	Stdev	Limit(U)	Limit(L)	Cp	Cpk	
10	193.5	128.8	64.7	164.7	23.2	900	200	5.03	-0.51	
Test Data										
	Measurement Position （mm）				Diagonal(μm)		Hardness	Conv.	Conv.	
No	X	Y	Distance	Load	D1	D2	HV	Scale	Hardness	Judge
1	3.186	1.004	3.34	200	53.3	54.01	128.8	HRC	0	OK
2	3.593	1.004	3.731	200	38.94	56	164.5	HRC	1.5	OK
3	3.891	1.187	4.068	200	39.23	48.32	193.5	HRC	9.3	OK
4	4.062	1.231	4.244	200	45.34	49.03	166.5	HRC	2.1	OK
5	3.859	1.626	4.188	200	44.34	49.03	170.1	HRC	3.1	OK

Table 10. Vickers Hardness Test for Carbon 0.75wt% Sample.

Statistics Data										
Point	Max.	Min.	R	Ave.	Stdev	Limit(U)	Limit(L)	Cp	Cpk	
10	139.7	93.5	46.2	105.3	19.5	900	200	6	-1.62	

Test Data										
	Measurement Position （ｍｍ）				Diagonal(μm)		Hardness	Conv.	Conv.	
No	X	Y	Distance	Load	D1	D2	HV	Scale	Hardness	Judge
1	-1.656	-7.797	7.971	200	62.11	58.84	101.4	HRC	0	OK
2	-1.399	-7.797	7.922	200	62.68	62.54	94.6	HRC	0	OK
3	-0.265	-7.518	7.523	200	58.84	67.08	93.5	HRC	0	OK
4	-0.019	-7.443	7.443	200	58.27	65.09	97.4	HRC	0	OK
5	0.27	-7.371	7.376	200	49.46	53.58	139.7	HRC	0	OK

1

2 Table 11. Vickers Hardness Test for Carbon 1.25wt% Sample.

Statistics Data										
Point	Max.	Min.	R	Ave.	Stdev	Limit(U)	Limit(L)	Cp	Cpk	
10	126.1	102.8	23.3	116.7	9.7	900	200	11.97	-2.85	
Test Data										
	Measurement Position （ｍｍ）				Diagonal(μm)		Hardness	Conv.	Conv.	
No	X	Y	Distance	Load	D1	D2	HV	Scale	Hardness	Judge
1	3.889	0.269	3.898	200	49.46	66.37	110.5	HRC	0	OK
2	3.219	0.206	3.226	200	57.42	62.68	102.8	HRC	0	OK
3	3.31	0.378	3.332	200	48.75	59.69	126.1	HRC	0	OK
4	3.31	0.604	3.365	200	54.43	55.14	123.5	HRC	0	OK
5	3.354	1.004	3.501	200	51.88	59.12	120.4	HRC	0	OK

3

4 Table 12. Vickers Hardness Test for Basalt 0.25wt% Sample

Statistics Data										
Point	Max.	Min.	R	Ave.	Stdev	Limit(U)	Limit(L)	Cp	Cpk	
10	243.6	194.2	49.4	219.9	20.3	900	200	5.75	0.33	
Test Data										
	Measurement Position （ｍｍ）				Diagonal(μm)		Hardness	Conv.	Conv.	
No	X	Y	Distance	Load	D1	D2	HV	Scale	Hardness	Judge
1	0.025	-0.04	0.047	200	37.95	42.07	231.6	HRC	18.4	OK
2	0.153	-0.115	0.191	200	35.96	42.07	243.6	HRC	21.1	OK
3	0.723	-0.115	0.732	200	40.08	45.19	204	HRC	12	OK
4	0.864	-0.147	0.876	200	39.65	41.36	226	HRC	17	OK
5	0.997	-0.22	1.021	200	40.93	46.47	194.2	HRC	9.5	OK

5

6 Table 13. Vickers Hardness Test for Basalt 0.75wt%

Statistics Data										
Point	Max.	Min.	R	Ave.	Stdev	Limit(U)	Limit(L)	Cp	Cpk	
10	278	76.4	201.6	189.4	76.1	900	200	1.53	-0.05	
Test Data										
	Measurement Position （ｍｍ）				Diagonal(μm)		Hardness	Conv.	Conv.	
No	X	Y	Distance	Load	D1	D2	HV	Scale	Hardness	Judge
1	2.082	0.309	2.105	200	36.1	40.08	255.6	HRC	23.2	OK
2	2.395	0.195	2.403	200	31.98	41.07	278	HRC	26.8	OK
3	2.796	0.195	2.803	200	36.52	45.62	219.8	HRC	15.5	OK
4	3.112	0.195	3.118	200	47.18	46.9	167.6	HRC	2.4	OK
5	3.823	0.195	3.828	200	48.18	55.14	138.9	HRC	0	OK
6	4.086	0.225	4.092	100	48.32	50.17	76.4	HRC	0	OK

Table 14. Vickers Hardness Test for Basalt 1.25wt% Sample.

Statistics Data										
Point	Max.	Min.	R	Ave.	Stdev	Limit(U)	Limit(L)	Cp	Cpk	
10	225.2	120.1	105.1	155	43.5	900	200	2.68	-0.34	
Test Data										
	Measurement Position （ｍｍ）				Diagonal(μm)		Hardness	Conv.	Conv.	
No	X	Y	Distance	Load	D1	D2	HV	Scale	Hardness	Judge
1	-0.062	0.064	0.089	200	43.2	37.95	225.2	HRC	16.8	OK
2	0.223	0.071	0.234	200	46.19	48.32	166	HRC	2	OK
3	0.653	8.125	8.151	200	49.46	52.3	143.2	HRC	0	OK
4	0.902	0.41	0.991	200	55.71	55.43	120.1	HRC	0	OK
5	0.878	0.652	1.094	200	53.58	57.28	120.7	HRC	0	OK

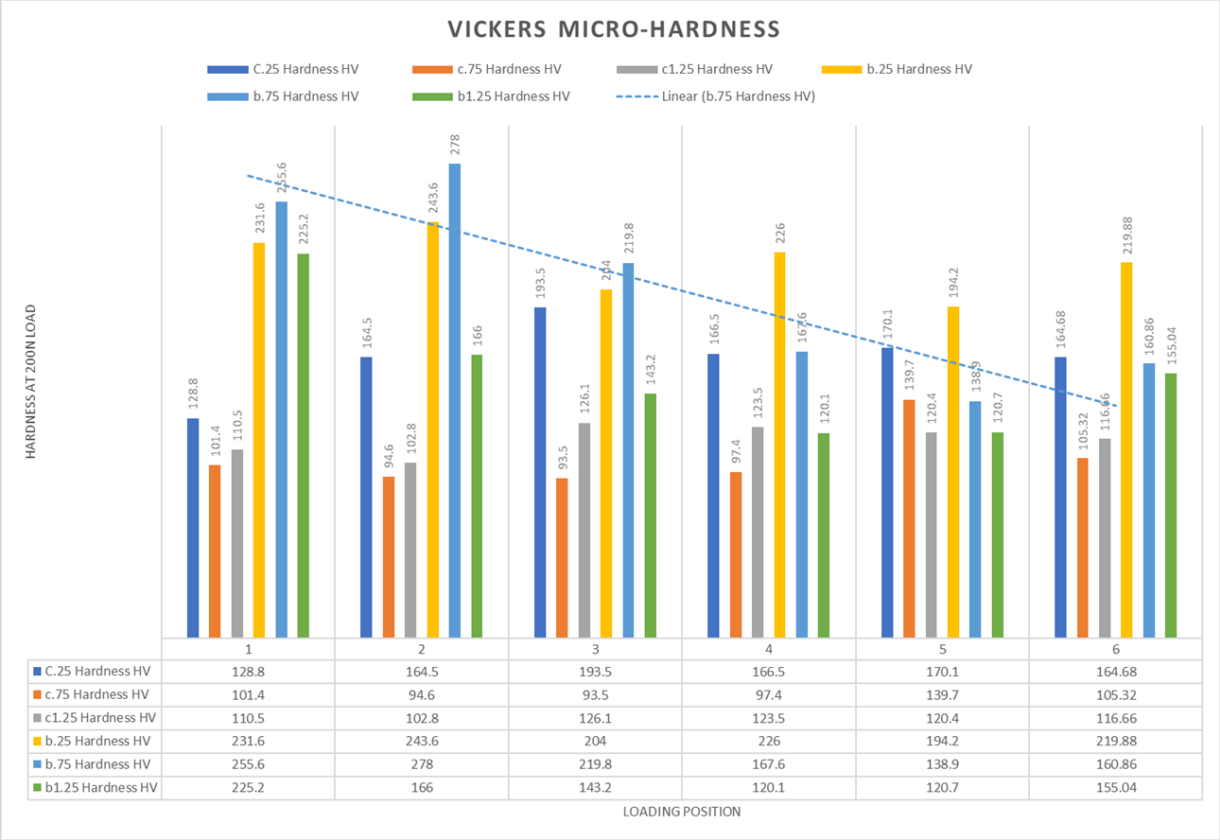

	1	2	3	4	5	6
C.25 Hardness HV	128.8	164.5	193.5	166.5	170.1	164.68
c.75 Hardness HV	101.4	94.6	93.5	97.4	139.7	105.32
c1.25 Hardness HV	110.5	102.8	126.1	123.5	120.4	116.66
b.25 Hardness HV	231.6	243.6	204	226	194.2	219.88
b.75 Hardness HV	255.6	278	219.8	167.6	138.9	160.86
b1.25 Hardness HV	225.2	166	143.2	120.1	120.7	155.04

Figure 16. Vickers Hardness Test Results

Figure 16 shows a graphical representation of the Vickers hardness test results for all the 6 samples as shown in Tables 8 to 13. The Basalt Fiber 0.25wt% and Basalt 0.75 have shown a consistent performance in the hardness test. Carbon has shown a rather inconsistent trends in hardness.

4.3. Pin on Disc Wear Test

This test was conducted using a DUCOM TR-201LE Pin on Disc Friction & Wear Testing Machine, for the 6 samples of Carbon & Basalt Fiber Reinforced Compact Sintered Samples. Each sample was tested on 450 rpm speed, and loads of 4 Kg. Before the test the disc was grinded, and cleaned with acetone to ensure appropriate reading, after each sample was tested for wear. The wear measurements were taken in microns. Figure 17 (a) to (f) shows all the graphs obtained in Pin on Disc wear tests for the samples, and Figure 17 (g) shows the setup.

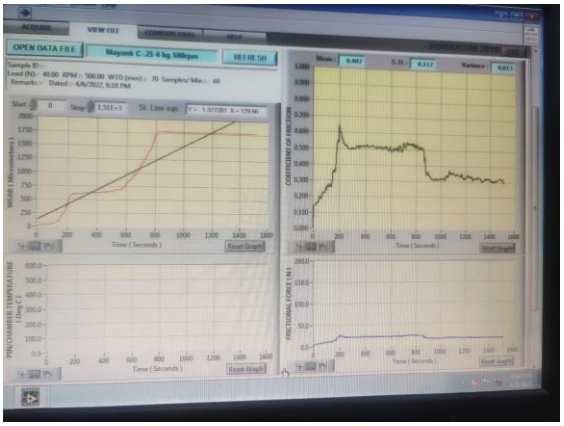

(a)

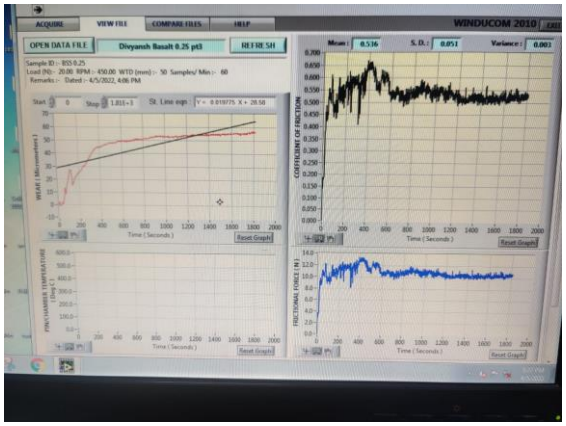

(b)

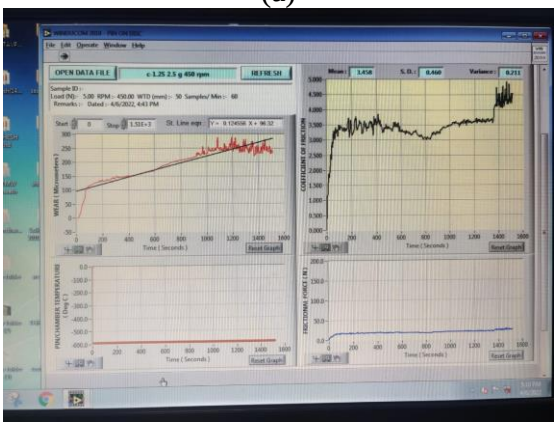

(c)

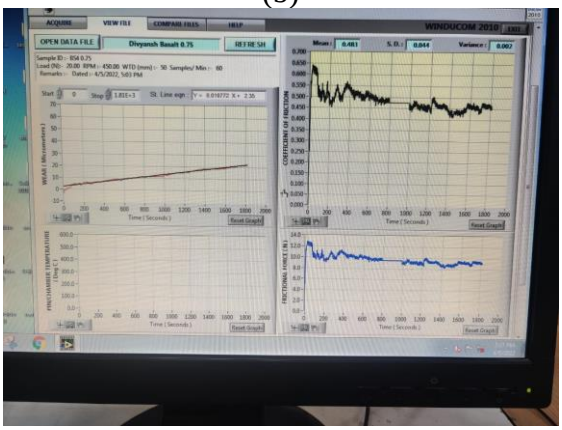

(d)

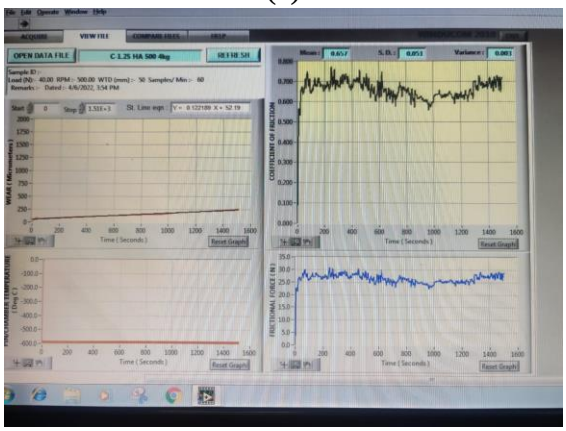

(e)

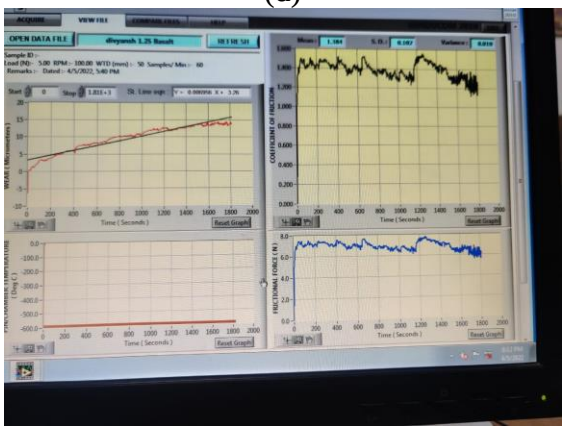

(f)

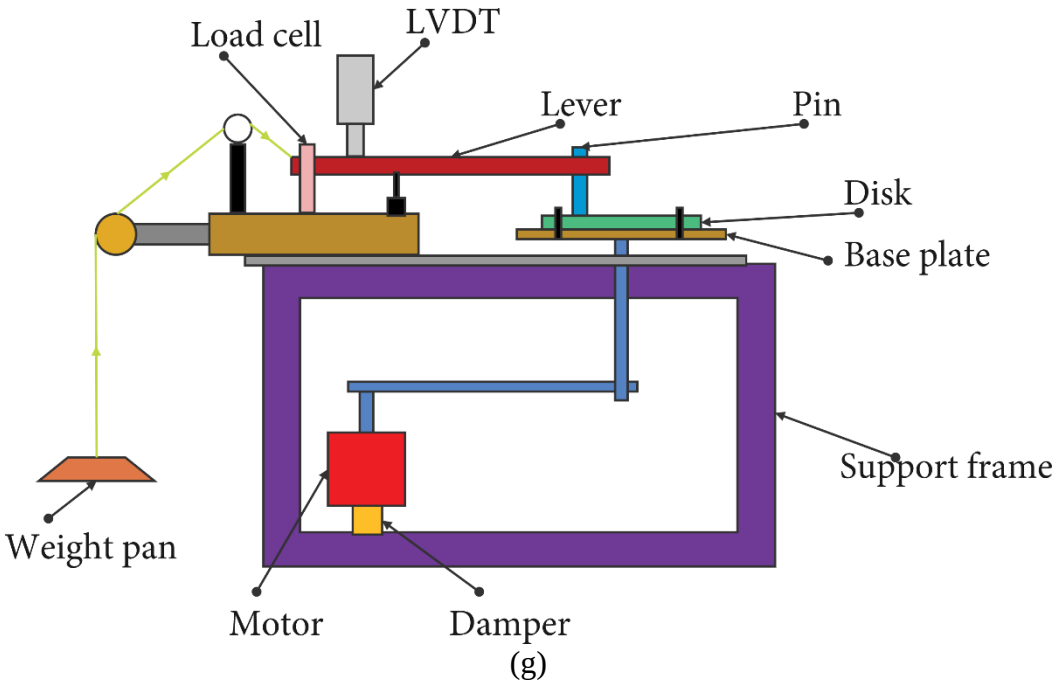

Figure 17. Pin on Disc Wear Test (a) C0.25wt%, (b) B0.25wt%, (c) C0.75wt%, (d) B0.75wt%, (e) C1.25wt%, (f) B1.25wt%, (g) Pin-on Disc Test Setup Illustration [14].

In the pin on disc wear test Basalt 0.25wt%, Basalt 0.75wt%, and Carbon 1.25wt% have shown the best result and a stable graph, visible in Figure 17 (b, d, e).

5. Conclusions

Basalt 0.25 wt% sample has shown a consistent performance in various tests, and the best performing sample reported. Basalt 0.75 wt% sample had the best results in some tests. Due to the inconsistent results of Basalt 0.75wt% samples in multiple iterations, but comparatively better performance than the samples with Carbon Fibers reinforced in the Copper Matrix. Vicker's hardness test and Pin on Disc wear tests show that the most consistent reading obtained is for the Basalt 0.25wt% has been much more consistent than for Basalt 0.75wt% and Carbon 1.25wt% samples.

Now, based on the XRD analysis and Pin on Disc Wear Test, Figure 18 shows two graphs for Carbon and Basalt Fiber based Copper samples' performance. Basalt samples have a divergent graphs, whereas carbon samples show consistency in wear. The graph is intended to display the longevity of the samples during wear based on the tests conducted.

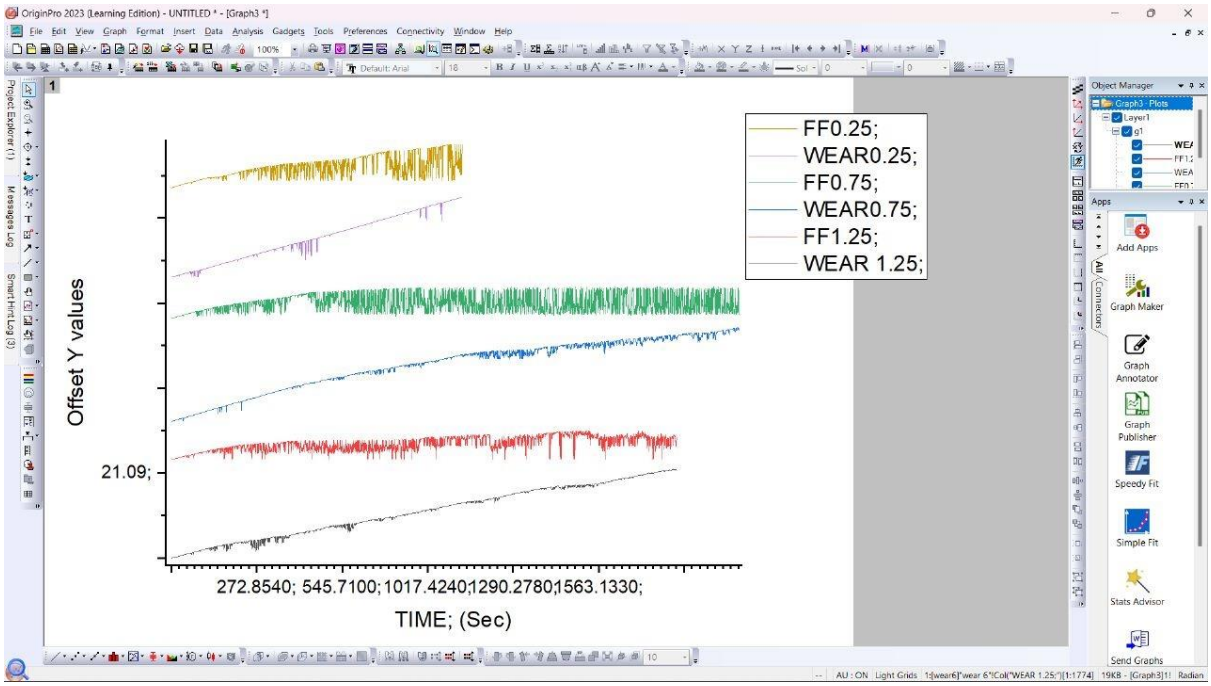

(a)

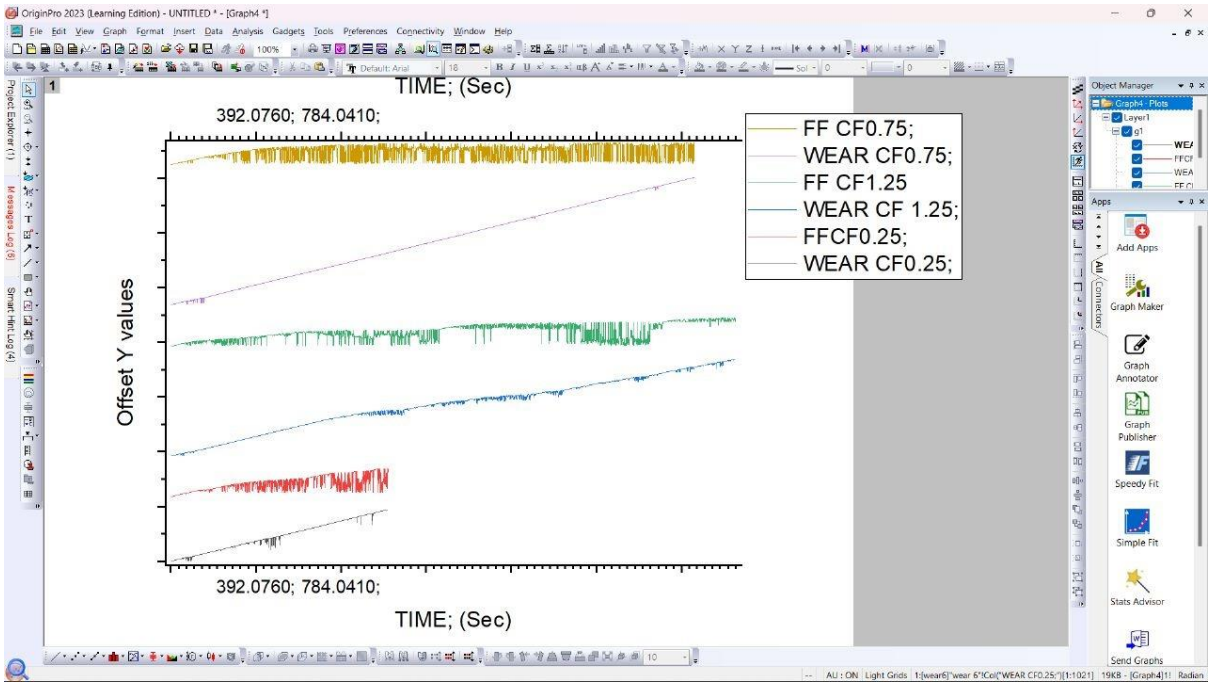

(b)

Figure 18. Time vs Wear Graph (a) Basalt Fiber (b) Carbon Fiber.

There was noise reported during the pin-on-disc wear test, which must be controlled. Copper is known for noise reduction while braking, but the Cu content being around 60-65%, there is a possibility of adding a small amount of additives to this recipe to control it because increasing copper will decrease the attained strength after reinforcing the fibers.

There is a possibility for experimentations of various other fibers compatible for increasing the strength of the Cu or any other matrix for braking, which can be vegetable or plant-based natural fibers as conducted by V. Vineeth Kumar et al. (2020) [23].

Declaration of Interests

The authors declare no conflict of interests.

Data Availability

Data is available upon reasonable request to the authors.

Funding

This research received no funding.

References

1. Rajan, B. S., Balaji, M. A. S., Sathickbasha, K., & Hariharasakthisudan, P. (2018). Influence of binder on thermomechanical and tribological performance in brake pad. Tribology in industry, 40(4), 654.
2. Kumar, S., & Ghosh, S. K. (2020). Porosity and tribological performance analysis on new developed metal matrix composite for brake pad materials. Journal of Manufacturing Processes, 59, 186-204.
3. Saikrishnan, G., Jayakumari, L. S., & Vijay, R. (2019). Influence of Iron–aluminum alloy on the tribological performance of non-asbestos brake friction materials–a solution for copper replacement. Industrial Lubrication and Tribology.
4. Hwang, H. J., Jung, S. L., Cho, K. H., Kim, Y. J., & Jang, H. (2010). Tribological performance of brake friction materials containing carbon nanotubes. Wear, 268(3-4), 519-525.
5. Vijay, R., Manoharan, S., & Nagarajan, S. (2020). Influence of premixed dual metal sulfides on the tribological performance of copper-free brake friction materials. Industrial Lubrication and Tribology.
6. Ahmed, K. A., Mohideen, S. R., Balaji, M. A. S., & Rajan, B. S. (2020). Tribological performance of brass powder with different copper and zinc content in the brake pad. Tribology in Industry, 42(2), 177.
7. Österle, W., Urban, I., Severin, D., & Trepte, S. (2001). Correlations between surface modification and tribological performance of brake pads. Surface engineering, 17(2), 123-125.
8. Dhanalakshmi, S., Sivakumar, P., Anil Kumar, V. N., & Raghavendra Bhat, R. (2007). Development and characterisation of copper based brake pads for armoured fighting vehicles. In National conference on automotive manufacturing, held at PSG College of Technology, Coimbatore, Organised by SAE India Southern Section.

9. Zhang, P., Zhang, L., Fu, K., Wu, P., Cao, J., Shijia, C., & Qu, X. (2019). The effect of Al2O3 fiber additive on braking performance of copper-based brake pads utilized in high-speed railway train. Tribology International, 135, 444-456.
10. Zhang, P., Zhang, L., Wu, P., Cao, J., Shijia, C., Wei, D., & Qu, X. (2020). Effect of carbon fiber on the braking performance of copper-based brake pad under continuous high-energy braking conditions. Wear, 458, 203408.
11. Zhang, P., Zhang, L., Wei, D., Wu, P., Cao, J., Shijia, C., & Qu, X. (2020). A high-performance copper-based brake pad for high-speed railway trains and its surface substance evolution and wear mechanism at high temperature. Wear, 444, 203182.
12. Ma, X., Luan, C., Fan, S., Deng, J., Zhang, L., & Cheng, L. (2021). Comparison of braking behaviors between iron-and copper-based powder metallurgy brake pads that used for C/C–SiC disc. Tribology International, 154, 106686.
13. Kalel, N., Bhatt, B., Darpe, A., & Bijwe, J. (2021). Copper-free brake-pads: A break-through by selection of the right kind of stainless steel particles. Wear, 464, 203537.
14. Selvaraj, S. K., Ramesh, R., Narendhra, T., Agarwal, I. N., Chadha, U., Paramasivam, V., & Palanisamy, P. (2021). New developments in carbon-based nanomaterials for automotive brake pad applications and future challenges. Journal of Nanomaterials, 2021.
15. Xiao, Y., Zhang, Z., Yao, P., Fan, K., Zhou, H., Gong, T., ... & Deng, M. (2018). Mechanical and tribological behaviors of copper metal matrix composites for brake pads used in high-speed trains. Tribology International, 119, 585-592.
16. Selvaraj, S. K., Srinivasan, K., Chadha, U., Mishra, R., Arpit, K., Apurb, K., & Hu, Y. C. (2021). Contemporary progresses in ultrasonic welding of aluminum metal matrix composites. Frontiers in Materials, 8, 647112.
17. https://phys.org/news/2019-08-youre-tough-h-bn.html (Last Accessed: 13 March 2022)
18. Zhang, P., Zhang, L., Wei, D., Wu, P., Cao, J., Shijia, C., & Qu, X. (2020). Adjusting function of MoS2 on the high-speed emergency braking properties of copper-based brake pad and the analysis of relevant tribo-film of eddy structure. Composites Part B: Engineering, 185, 107779.
19. Ma, X., Luan, C., Fan, S., Deng, J., Zhang, L., & Cheng, L. (2021). Comparison of braking behaviors between iron-and copper-based powder metallurgy brake pads that used for C/C–SiC disc. Tribology International, 154, 106686.
20. https://www.counterman.com/low-no-copper-brake-pads-counter-pros-need-know/ (Last Accessed: 13 March 2022)
21. Mandal, S., Sanyal, A. S., Dhargupta, K. K., & Ghatak, S. (2001). Gas pressure sintering of β SiC–γ-AlON composite in nitrogen/argon environment. Ceramics international, 27(4), 473-479.
22. Yu, E. K., Piao, L., & Kim, S. H. (2011). Sintering behavior of copper nanoparticles. Bulletin of the Korean Chemical Society, 32(11), 4099-4102.
23. Vineeth Kumar V. & Senthil Kumaran S. (2020): Characterization of Various Properties of Chemically Treated Alliumsativum Fiber for Brake Pad Application, Journal of Natural Fibers, DOI: 10.1080/15440478.2020.1745130
24. Zhang, S., Hao, Q., Liu, Y., Jin, L., Ma, F., Sha, Z., & Yang, D. (2018). Simulation Study on Friction and Wear Law of Brake Pad in High-Power Disc Brake. *Mathematical Problems in Engineering*, *2019*(1), 6250694. https://doi.org/10.1155/2019/6250694

Appendix A: Simulation Outcomes in an AFV's Conditions

The thermal analysis for the brake pad samples was conducted using Fusion 360. For the simulations, the materials were assigned in the manner as mentioned in the Tables A, B. After assigning these properties to the CAD model, there were further investigations conducted for thermal analysis & performance assessment.

Table A. Cu Matrix with Reinforced Carbon Fiber.

S.no.	material	wt%	property									
			Poission's ratio (Theoretical/Actual)		Shear modulus (Theoretical/Actual)		Tensile Strength (Theoretical/Actual)		Young's modulus (Theoretical/Actual)		Density (Theoretical/Actual)	
1	Cu	62	0.34	0.2108	44	27.28	210	130.2	121	75.02	8.96	5.5552
2	Fe1	8	0.29	0.0232	78	6.24	230	18.4	204	16.32	7.874	0.62992
3	CrFe	10	0.5	0.05	80	8	243	24.3		0	7.6	0.76
4	SiC	7	0.35	0.0245	32	2.24	240	16.8	90	6.3	3.21	0.2247
5	BN	10	0.211	0.0211	5.83	0.583	82	8.2	865	86.5	2.1	0.21
6	MoS2	2.75	0.25	0.006875	184	5.06	265	7.2875	330	9.075	5.06	0.13915
7	C Fiber	0.25	0.23	0.000575	3	0.0075	5	0.0125	85	0.2125	1.6	0.004
Total		100	2.171	0.33705	426.83	49.4105	1275	205.2	1695	193.4275	36.404	7.52297

Table B. Cu Matrix with Reinforced Basalt Fiber

S.no.	material	wt%	property									
			Poission's ratio		Shear modulus		Tensile Strength		Young's modulus		Density	
1	Cu	62	0.34	0.2108	44	27.28	210	130.2	121	75.02	8.96	5.5552
2	Fe1	8	0.29	0.0232	78	6.24	230	18.4	204	16.32	7.874	0.62992
3	CrFe	10	0.5	0.05	80	8	243	24.3	400	40	7.6	0.76
4	SiC	7	0.35	0.0245	32	2.24	240	16.8	90	6.3	3.21	0.2247
5	BN	10	0.211	0.0211	5.83	0.583	83.3	8.33	865	86.5	2.1	0.21
6	MoS2	2.75	0.25	0.006875	184	5.06	265	7.2875	330	9.075	5.06	0.13915
7	B Fiber	0.25	0.23	0.000575	15	0.0375	3	0.0075	92	0.23	2.67	0.006675
Total		100	2.171	0.33705	438.83	49.4405	1274.3	205.325	2102	233.445	37.474	7.525645

The below cases shown are for the amount of force applied in an AFV's environment, and it explains the application of the force, the possible displacements happening under various loads.

Following are the assumptions considered for detecting displacement with constant temperature:

1. The contact surface between the friction components is perfectly flat.
2. The frictional behavior follows Coulomb's law, with a constant friction coefficient during the braking process.
3. The heat produced by friction on both the inner and outer sides of the brake pad is equal, thus only one side of the brake disc is analyzed.
4. The instantaneous temperature at corresponding points on the contact surfaces of the brake disc and brake pad is the same.

5. The pressure distribution across the brake pad is uniform.
6. The materials of the brake disc and brake pad are isotropic. Due to the brief duration of emergency braking, the thermal properties of the materials are considered constant and do not vary with temperature. [24]

Thermal Plots for Analysis

Based on the results the thermal material properties estimated, we could simulate Thermal properties of the material, with graphs for Specific Heat (Plot 1), Thermal Conductivity (Plot 2) and Thermal Expansion Coefficient (Plot 3).

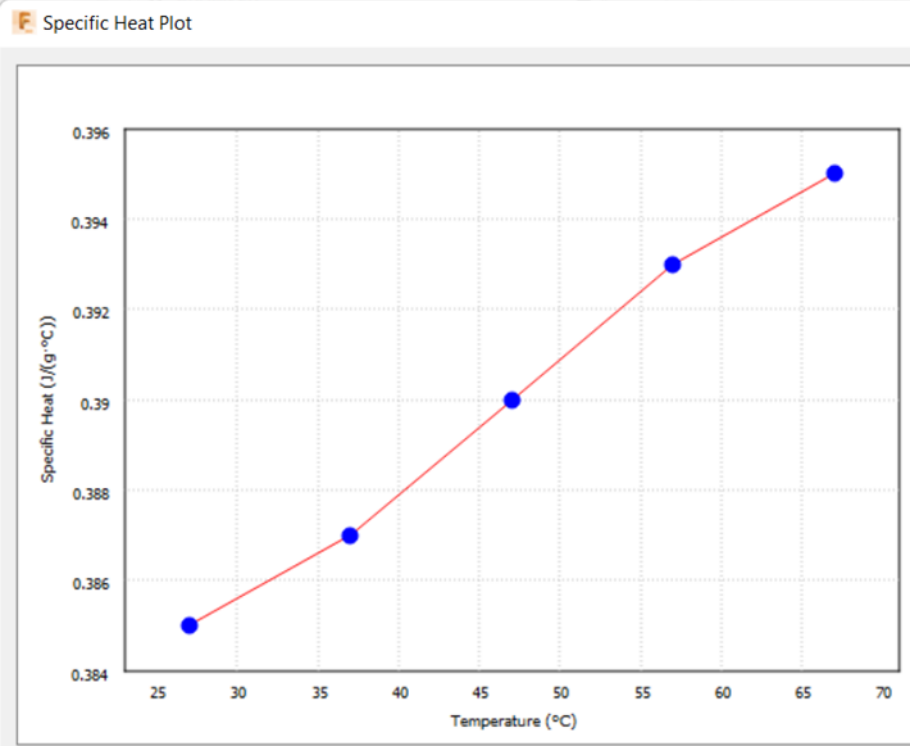

Plot 1. Specific Heat Plot

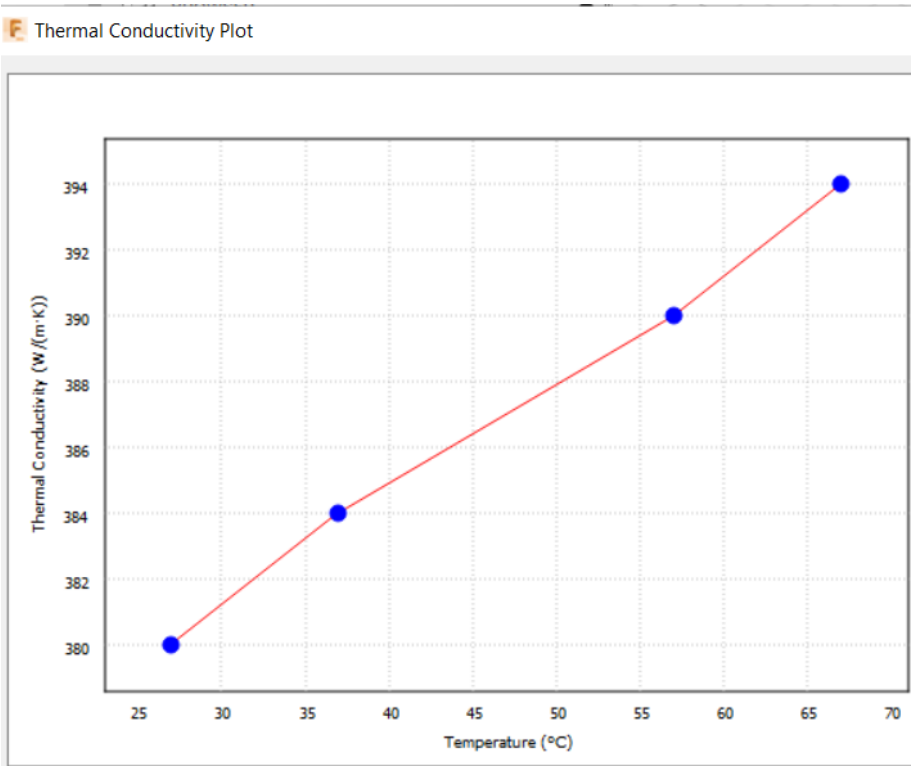

Plot 2. Thermal Conductivity Plot

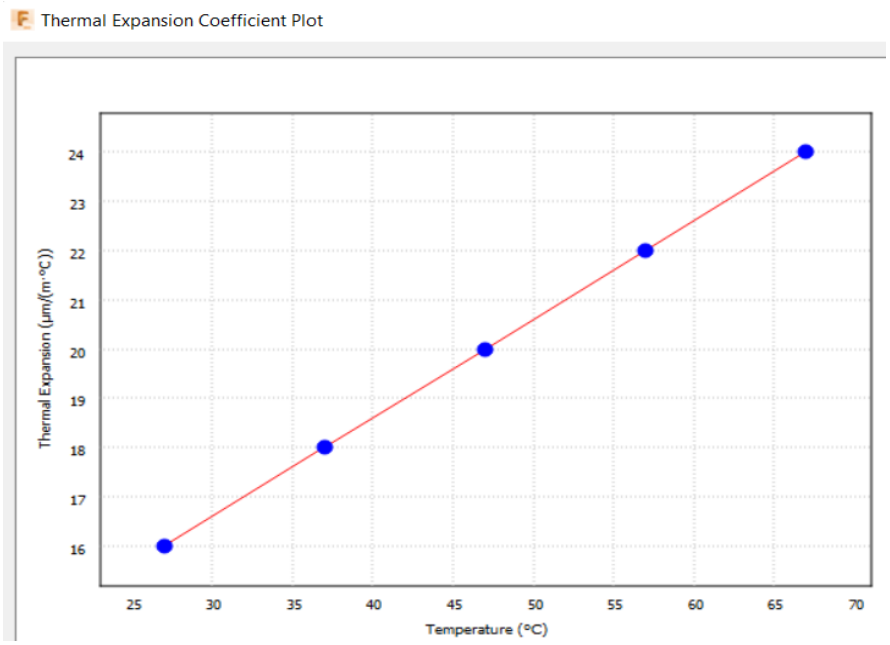

Plot 3. Thermal Expansion Coefficient Plot

With the data points of the brake pad material and by using the Johnson-Cook model that effectively captures the softening effects due to strain rate and temperature rise, making it highly applicable in finite element simulations. This model represents the combined influence of strain, strain rate, and temperature through a multiplicative relationship. [24]

$$\sigma_e = \left[A + B\left(\varepsilon_e^p\right)^n\right]\left[1 + Cln\,\frac{\varepsilon_e^p}{\varepsilon_o}\right]\left[1 - \left(\frac{T - T_{room}}{T_{melt} - T_{room}}\right)^m\right]$$

Table C: Material parameters for Johnson-Cook Model.

Brake pad material type	Density	Thermal Conductivity	Poisson's Ratio	Linear Expansion Coefficient	Specific Heat Capacity	Young's Modulus
Carbon Fibre	36.404	380	0.33705	16	0.385	1695
Basalt Fibre	37.474	380	0.33705	16	0.385	2102

Based on the conclusion we found Basalt 25% by weight to perform the most consistant and hence in order to test the viability of a brake pad made of such material, Finite Element Simulations were performed, in a case by case format with varying force applied by the caliper on the disk brake during normal operations. To visualize the deformation and wear while braking.

CASE I: 2 Tonnes Force.

A force of 2 tonnes is applied radially In to mimic the compression force endured by the brake pad during Braking phase. In Case I we can observe a deflection of 0.02678mm compression between 2 opposite set of brake pads.

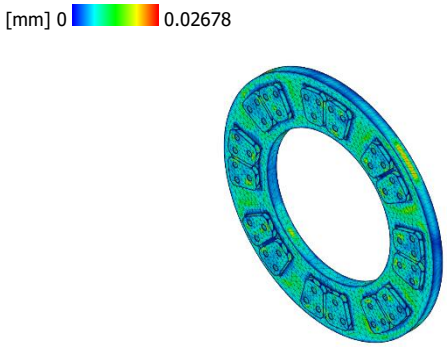

Table C. Simulations Outcomes for 2 Tonnes Force.

Name	Minimum	Maximum
Safety Factor		
Safety Factor (Per Body)	0.06993	15
Stress		
Von Mises	0.3606 MPa	3276 MPa
1st Principal	-785.8 MPa	4564 MPa
3rd Principal	-1447 MPa	4361 MPa
Normal XX	-1254 MPa	4400 MPa
Normal YY	-954.2 MPa	4505 MPa
Normal ZZ	-1125 MPa	4436 MPa
Shear XY	-1745 MPa	1720 MPa
Shear YZ	-1724 MPa	1738 MPa
Shear ZX	-1127 MPa	1036 MPa
Displacement		
Total	0 mm	0.02678 mm
X	-0.02376 mm	0.02397 mm
Y	-0.01978 mm	0.01858 mm
Z	-0.02383 mm	0.02208 mm
Reaction Force		
Total	0 N	926723 N
X	-57612 N	72425 N
Y	-926639 N	676227 N
Z	-65638 N	52631 N
Strain		
Equivalent	2.409E-06	0.02422
1st Principal	-9.024E-04	0.02506
3rd Principal	-0.02315	5.451E-04
Normal XX	-0.01332	0.004765
Normal YY	-0.01078	0.006107
Normal ZZ	-0.01213	0.00476
Shear XY	-0.02015	0.01994
Shear YZ	-0.02002	0.01998
Shear ZX	-0.01208	0.0111
Contact Pressure		
Total	0 MPa	3067 MPa
X	-1997 MPa	2008 MPa
Y	-3067 MPa	2549 MPa
Z	-2000 MPa	2029 MPa
Temperature		
Temperature	66.81 C	66.94 C
Heat Flux		

We can observe the displacement in X axis in the range of -0.02376mm to 0.02397mm; in Y axis in the range of -0.01978mm to 0.01858; and Z axis in the range of -0.02383 to 0.02208; with the net deviation of 0.02678mm.

CASE II: 2.5 Tonnes Force.

A force of 2.5 tonnes is applied radially In to mimic the compression force endured by the brake pad during Braking phase. In Case II we can observe a deflection of 0.02678mm compression between 2 opposite set of brake pads.

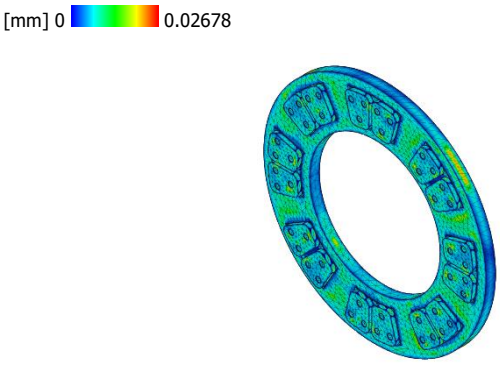

Table D. Simulations Outcomes for 2.5 Tonnes Force.

Name	Minimum	Maximum
Safety Factor		
Safety Factor (Per Body)	0.06993	15
Stress		
Von Mises	0.3606 MPa	3276 MPa
1st Principal	-785.8 MPa	4565 MPa
3rd Principal	-1447 MPa	4361 MPa
Normal XX	-1254 MPa	4400 MPa
Normal YY	-954.2 MPa	4505 MPa
Normal ZZ	-1125 MPa	4436 MPa
Shear XY	-1745 MPa	1720 MPa
Shear YZ	-1724 MPa	1738 MPa
Shear ZX	-1127 MPa	1036 MPa
Displacement		
Total	0 mm	0.02678 mm
X	-0.02376 mm	0.02397 mm
Y	-0.01978 mm	0.01858 mm
Z	-0.02383 mm	0.02208 mm
Reaction Force		
Total	0 N	926707 N
X	-57613 N	72427 N
Y	-926623 N	676216 N
Z	-65640 N	52633 N
Strain		
Equivalent	2.409E-06	0.02422
1st Principal	-9.024E-04	0.02506
3rd Principal	-0.02315	5.451E-04
Normal XX	-0.01332	0.004765
Normal YY	-0.01078	0.006107
Normal ZZ	-0.01213	0.00476
Shear XY	-0.02015	0.01994
Shear YZ	-0.02002	0.01998
Shear ZX	-0.01209	0.0111
Contact Pressure		
Total	0 MPa	3067 MPa
X	-1997 MPa	2008 MPa
Y	-3067 MPa	2549 MPa
Z	-2000 MPa	2029 MPa
Temperature		
Temperature	66.81 C	66.94 C
Heat Flux		

We can observe the displacement in X axis in the range of -0.02376mm to 0.02397mm; in Y axis in the range of -0.01978mm to 0.01858; and Z axis in the range of -0.02383 to 0.02208; with the net deviation of 0.02678mm.

Case III: 3 Tonnes Force.

A force of 3 tonnes is applied radially In to mimic the compression force endured by the brake pad during Braking phase. In Case III we can observe a deflection of 0.02676mm compression between 2 opposite set of brake pads.

[mm] 0 0.02676

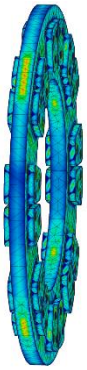

Table E. Simulation Outcomes for 3 Tonnes Force.

Name	Minimum	Maximum
Safety Factor		
Safety Factor (Per Body)	0.0699	15
Stress		
Von Mises	0.3608 MPa	3271 MPa
1st Principal	-791.4 MPa	4567 MPa
3rd Principal	-1450 MPa	4363 MPa
Normal XX	-1258 MPa	4403 MPa
Normal YY	-955.1 MPa	4507 MPa
Normal ZZ	-1130 MPa	4438 MPa
Shear XY	-1741 MPa	1716 MPa
Shear YZ	-1720 MPa	1734 MPa
Shear ZX	-1129 MPa	1037 MPa
Displacement		
Total	0 mm	0.02676 mm
X	-0.02366 mm	0.02386 mm
Y	-0.01977 mm	0.01854 mm
Z	-0.02372 mm	0.02196 mm
Reaction Force		
Total	0 N	928462 N
X	-57758 N	72603 N
Y	-928379 N	677462 N
Z	-65798 N	52721 N
Strain		
Equivalent	2.41E-06	0.02423
1st Principal	-9.012E-04	0.02503
3rd Principal	-0.02316	5.463E-04
Normal XX	-0.01333	0.004776
Normal YY	-0.0108	0.006117
Normal ZZ	-0.01214	0.004771

We can observe the displacement in X axis in the range of -0.02366mm to 0.02386mm; in Y axis in the range of -0.01977mm to 0.01854; and Z axis in the range of -0.02372 to 0.02196; with the net deviation of 0.02676mm.

CASE IV: 5 Tonnes Forces

A force of 5 tonnes is applied radially In to mimic the compression force endured by the brake pad during Braking phase. In Case IV we can observe a deflection of 0.02673mm compression between 2 opposite set of brake pads.

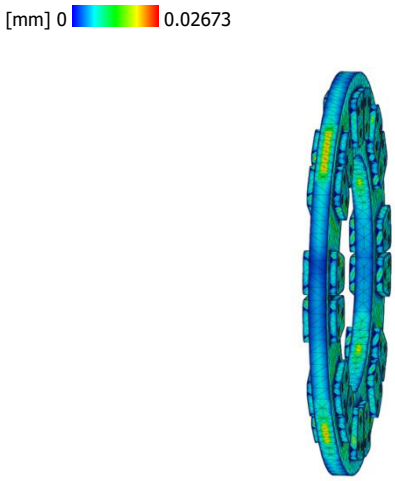

Table F. Simulation Outcomes for 5 Tonnes Force.

Name	Minimum	Maximum
Safety Factor		
Safety Factor (Per Body)	0.06986	15
Stress		
Von Mises	0.3611 MPa	3263 MPa
1st Principal	-799.6 MPa	4571 MPa
3rd Principal	-1455 MPa	4366 MPa
Normal XX	-1263 MPa	4406 MPa
Normal YY	-956.6 MPa	4511 MPa
Normal ZZ	-1137 MPa	4441 MPa
Shear XY	-1736 MPa	1710 MPa
Shear YZ	-1714 MPa	1728 MPa
Shear ZX	-1131 MPa	1038 MPa
Displacement		
Total	0 mm	0.02673 mm
X	-0.02351 mm	0.02368 mm
Y	-0.01975 mm	0.01848 mm
Z	-0.02355 mm	0.02179 mm
Reaction Force		
Total	0 N	930977 N
X	-57967 N	72857 N
Y	-930894 N	679250 N
Z	-66027 N	52847 N
Strain		
Equivalent	2.412E-06	0.02424
1st Principal	-8.993E-04	0.02499
3rd Principal	-0.02317	5.481E-04
Normal XX	-0.01334	0.004792
Normal YY	-0.01083	0.006131
Normal ZZ	-0.01214	0.004788
Shear XY	-0.02017	0.01996
Shear YZ	-0.02004	0.01999
Shear ZX	-0.01213	0.01113
Contact Pressure		
Total	0 MPa	3064 MPa
X	-1999 MPa	2010 MPa
Y	-3064 MPa	2551 MPa
Z	-2002 MPa	2031 MPa
Temperature		
Temperature	68.58 C	68.72 C
Heat Flux		
Total	6.661E-07 W / mm^2	0.001855 W / mm^2
X	-9.981E-04 W / mm^2	9.384E-04 W / mm^2
Y	-0.001849 W / mm^2	0.001741 W / mm^2
Z	-0.001017 W / mm^2	8.967E-04 W / mm^2
Thermal Gradient		
Total	1.48E-05 C / mm	0.01582 C / mm
X	-0.008248 C / mm	0.008132 C / mm
Y	-0.015 C / mm	0.01439 C / mm
Z	-0.008142 C / mm	0.008292 C / mm
Applied Heat Flow		
Applied Heat Flow	-1.661E-09 W / mm^2	1.795E-07 W / mm^2

We can observe the displacement in X axis in the range of -0.02351mm to 0.02368mm; in Y axis in the range of -0.01975mm to 0.01848; and Z axis in the range of -0.02355 to 0.02179mm; with the net deviation of 0.02673mm.

Temperature & Displacement

Case I: 2 Tonnes Force.

Due to friction during the Braking Process a lot of heat is generated as the caliper grabs the brake pads, when a braking force of 2 Tonnes is applied during regular operation we can observe heat generated to 66.81 - 66.94℃

Temp and Displacement at 2 tonne Force

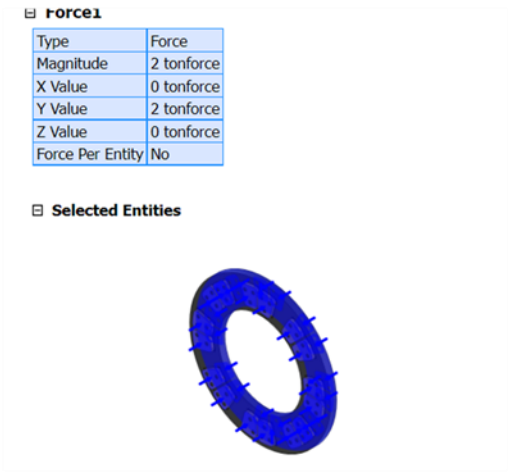

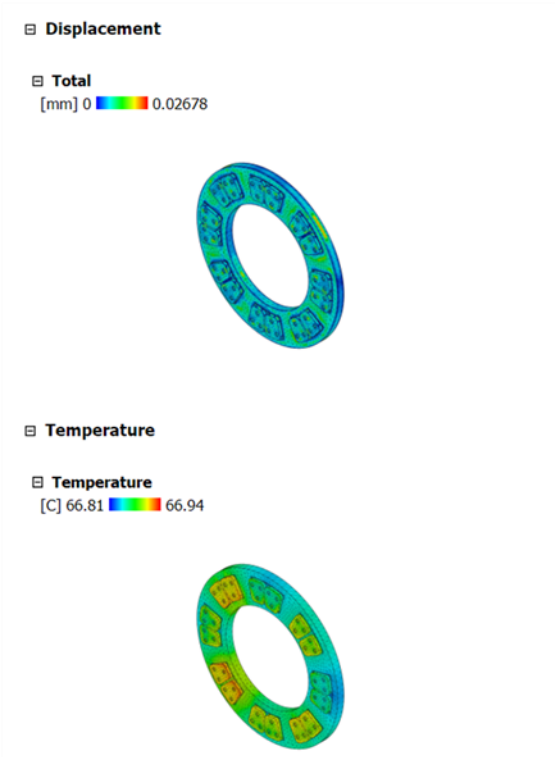

Case II: 2.5 Tonnes Force

when a force of 2.5 Tonnes is applied during regular operation, we can observe the readings don't change and the heat generated to 66.81 - 66.94℃

Temp and Displacement at 2.5 tonne Force

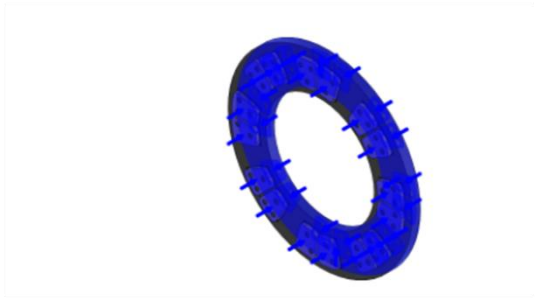

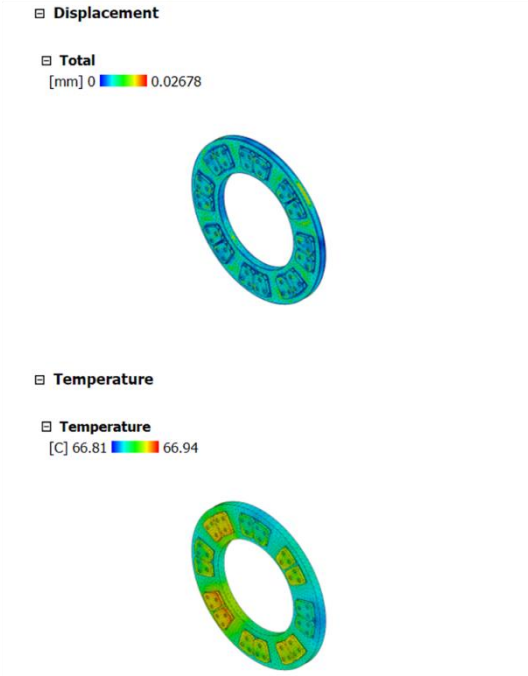

Case III: 3 Tonnes Force.

when a force of 3 Tonnes is applied during regular operation, we can observe heat generated to 67.52 - 67.66℃

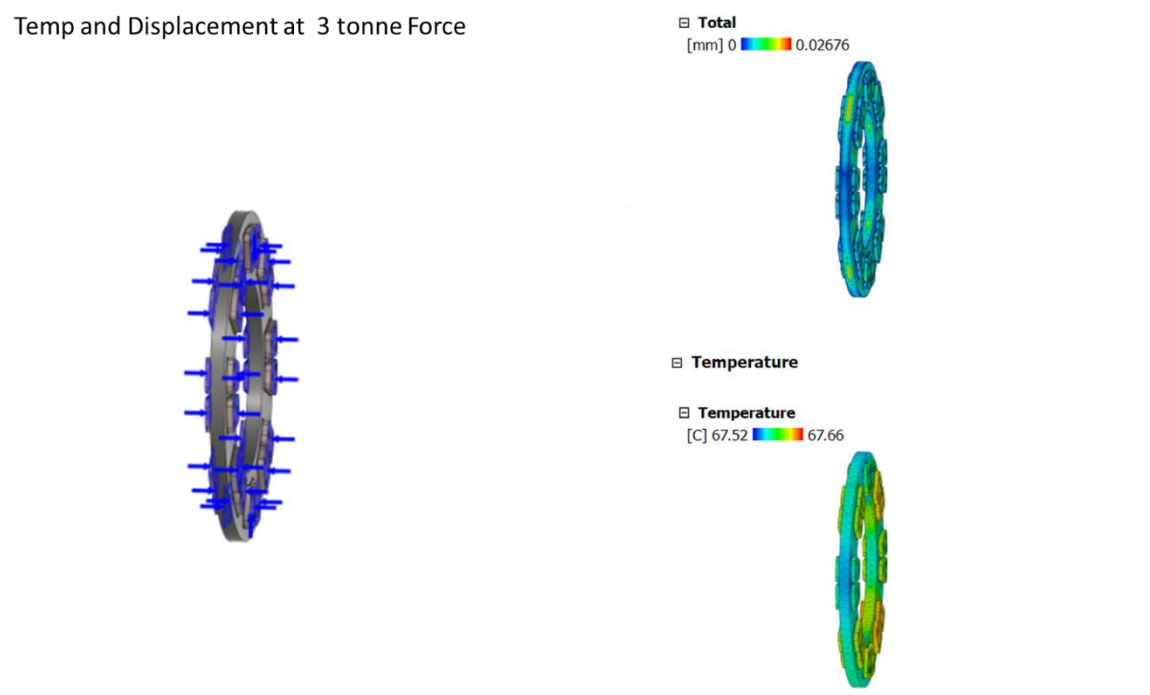

Case IV: 5 Tonnes Force.

when a force of 3 Tonnes is applied during regular operation, we can observe heat generated to 68.58 – 68.72℃

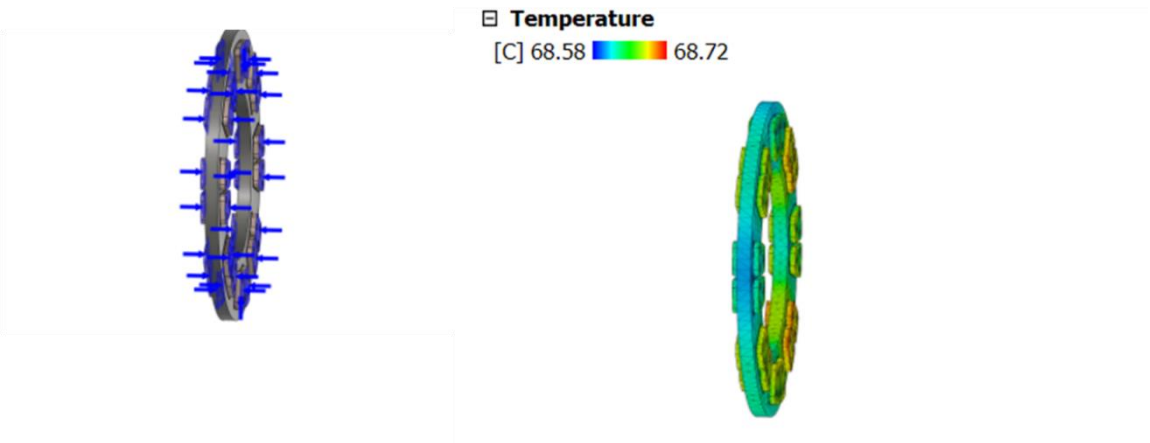

The brake pad and brake disc elements press against each other, deforming the mesh elements and resulting in a non-flat brake disc surface. Braking friction also affects the rough surface, producing rough peaks on the deformed disc. These rough peaks compress during relative motion, causing shear deformation and wear. This combination intensifies material deformation, increasing contact pressure and local temperatures, which in turn exacerbates wear. The wear depth is greater at the edge of the friction inlet. Conversely, the intermediate region, being farther from the friction edge and subject to lower pressing forces, shows minimal material deformation and lower friction heat, resulting in less wear. In the brake pad's central area, wear depth initially increases slowly and then sharply with temperature and pressure changes. Due to the brake disc's heat conduction, the friction outlet temperature of the brake pad is high, leading mainly to adhesive wear, which makes the friction surface rough due to the transfer of friction material.